Global Biogeochemical Cycles

RESEARCH ARTICLE
10.1029/2018GB006154

Pacific Anthropogenic Carbon Between 1991 and 2017

B. R. Carter[1,2], R. A. Feely[2], R. Wanninkhof[3], S. Kouketsu[4], R. E. Sonnerup[1], P. C. Pardo[5], C. L. Sabine[6], G. C. Johnson[2], B. M. Sloyan[7], A. Murata[4], S. Mecking[8], B. Tilbrook[9], K. Speer[10], L. D. Talley[11], F. J. Millero[12], S. E. Wijffels[7,13], A. M. Macdonald[13], N. Gruber[14], and J. L. Bullister[2,15]

[1]Joint Institute for the Study of the Atmosphere and Ocean, University of Washington, Seattle, WA, USA, [2]Pacific Marine Environmental Laboratory, National Oceanic and Atmospheric Administration, Seattle, WA, USA, [3]Atlantic Oceanographic and Meteorological Laboratory, National Oceanic and Atmospheric Administration, Miami, FL, USA, [4]Japan Agency for Marine-Earth Science and Technology (JAMSTEC), Yokosuka, Japan, [5]Antarctic Climate and Ecosystem Cooperative Research Center, University of Tasmania, Hobart, Tasmania, Australia, [6]SOEST, University of Hawaiʻi at Mānoa, Honolulu, HI, USA, [7]CSIRO Oceans and Atmosphere, Hobart, Tasmania, Australia, [8]Applied Physics Laboratory, University of Washington, Seattle, WA, USA, [9]Commonwealth Scientific and Industrial Research Organisation (CSIRO) Marine Research and Antarctic Climate and Ecosystem Cooperative Research Center, Hobart, Tasmania, Australia, [10]Department of Oceanography, The Florida State University, Tallahassee, FL, USA, [11]Scripps Institution of Oceanography, University of California, San Diego, La Jolla, CA, USA, [12]Rosenstiel School of Marine and Atmospheric Science, University of Miami, Coral Gables, FL, USA, [13]Woods Hole Oceanographic Institution, Woods Hole, MA, USA, [14]Environmental Physics, Institute of Biogeochemistry and Pollutant Dynamics, ETH Zurich, Zurich, Switzerland, [15]Deceased

Key Points:
- C_{anth} storage in the top 1,500 m of the Pacific increased from 0.88 +/-0.11 PgC/year from 1995 to 2005 to 1.17 +/-0.11 PgC/year from 2005 to 2015
- The high density and measurement quality of the current repeat hydrographic program is essential to directly assess decadal C_{anth} storage
- C_{anth} variability exceeds expectations from atmospheric CO_2 accumulation and may be comparable to total air-sea CO_2 flux variability

Supporting Information:
- Supporting Information S1
- Table S1

Correspondence to:
B. R. Carter,
brendan.carter@noaa.gov

Citation:
Carter, B. R., Feely, R. A., Wanninkhof, R., Kouketsu, S., Sonnerup, R. E., Pardo, P. C., et al. (2019). Pacific anthropogenic carbon between 1991 and 2017. *Global Biogeochemical Cycles*, *33*, 597–617. https://doi.org/10.1029/2018GB006154

Received 11 DEC 2018
Accepted 24 APR 2019
Accepted article online 29 APR 2019
Published online 31 MAY 2019

Abstract We estimate anthropogenic carbon (C_{anth}) accumulation rates in the Pacific Ocean between 1991 and 2017 from 14 hydrographic sections that have been occupied two to four times over the past few decades, with most sections having been recently measured as part of the Global Ocean Ship-based Hydrographic Investigations Program. The rate of change of C_{anth} is estimated using a new method that combines the extended multiple linear regression method with improvements to address the challenges of analyzing multiple occupations of sections spaced irregularly in time. The C_{anth} accumulation rate over the top 1,500 m of the Pacific increased from 8.8 ($\pm$1.1, 1σ) Pg of carbon per decade between 1995 and 2005 to 11.7 ($\pm$1.1) PgC per decade between 2005 and 2015. For the entire Pacific, about half of this decadal increase in the accumulation rate is attributable to the increase in atmospheric CO_2, while in the South Pacific subtropical gyre this fraction is closer to one fifth. This suggests a substantial enhancement of the accumulation of C_{anth} in the South Pacific by circulation variability and implies that a meaningful portion of the reinvigoration of the global CO_2 sink that occurred between ~2000 and ~2010 could be driven by enhanced ocean C_{anth} uptake and advection into this gyre. Our assessment suggests that the accuracy of C_{anth} accumulation rate reconstructions along survey lines is limited by the accuracy of the full suite of hydrographic data and that a continuation of repeated surveys is a critical component of future carbon cycle monitoring.

1. Introduction

CO_2 acts as a greenhouse gas that traps infrared radiation as observed at the top of the atmosphere (Loeb et al., 2012) and increases in the atmospheric concentration of carbon dioxide (CO_2) result in warming of the ocean, ground, and atmosphere and in phase changes of ice to liquid water and liquid water to water vapor. Humans are presently emitting approximately ~10 Pg of carbon (or PgC with Pg=10^{15}g) as CO_2 gas into the atmosphere every year. About half of the CO_2 released by humans has remained in the atmosphere (Ciais et al., 2019), while a smaller fraction—historically averaging 28% to 34% of human emissions—has been absorbed by the ocean (e.g., Gruber, Clement, et al., 2019; Le Quéré et al., 2016) where it reacts with water to form a weak acid that is mostly neutralized by carbonate ions. As a result, the surface ocean is becoming depleted in carbonate ions. The bicarbonate-carbonate ion pair forms the dominant acid-base buffer in seawater, and ocean CO_2 storage is leading to a decreased capacity of the ocean to store additional "anthropogenic" CO_2 (or C_{anth}; Sarmiento & Le Quéré, 1996). Ocean acidification from CO_2 uptake is lowering seawater pH and making the ocean more corrosive for shells and hard parts of marine organisms that are composed of calcium carbonate ($CaCO_3$) minerals (Doney et al., 2009; Gattuso et al., 2015; Orr et al., 2005).

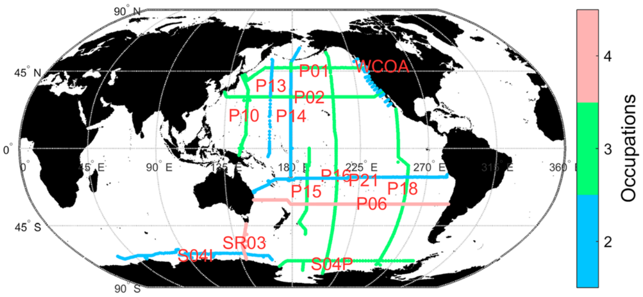

Figure 1. Map of the repeat hydrographic sections considered in this analysis color coded by the number of occupations with sufficient measurement density for analysis. Cruise information is provided in supporting information "CruiseInformation.xlsx." WCOA = West Coast Ocean Acidification.

Monitoring changes in the rate of C_{anth} storage in the oceans is critical for several reasons. First, in many efforts to establish global carbon budgets, changes in the net land carbon reservoir are estimated from residuals between anthropogenic emissions and changes in the CO_2 concentrations in the atmosphere and the oceans. Refining ocean C_{anth} storage estimates therefore improves our constraint for the global terrestrial carbon sink (Le Quéré et al., 2015). Second, understanding the modern C_{anth} distribution is important for quantifying how different modern ocean chemistry is from its preindustrial and paleo-oceanographic states (Zeebe, 2012). Third, accurate and time-varying C_{anth} distribution records are critical for assessing and validating carbon cycle models that simulate future atmospheric CO_2 under potential future emission scenarios (e.g., Caldeira & Wickett, 2005; Orr et al., 2001; Wang et al., 2012). Overall, it is important to know the size and spatial patterns of the ocean carbon sink and how they evolve over time.

The Pacific Ocean is a substantial sink for C_{anth} due to its large size. Per unit area, the Pacific Ocean is less efficient at storing C_{anth} than the Atlantic Ocean because the deep Pacific Ocean contains a substantial amount of water that has not been exposed to the atmosphere for thousands of years, whereas the deep Atlantic is exposed to the atmosphere through North Atlantic Deep Water formation on timescales closer to hundreds of years (England, 1995). Except for the portions of the abyssal Pacific ventilated by waters sinking along the Antarctic continental margin (e.g., Johnson, 2008; Orsi et al., 1999), the waters in the deep Pacific (below 2,000-m depth) have not been in contact with the atmosphere since long before human CO_2 emissions became substantial. Despite the slow ventilation of the deep Pacific, the Pacific Ocean stores as much or more C_{anth} than any other ocean basin (i.e., about 37% to 42% of the total ocean storage; Gruber, Clement, et al., 2019; Sabine et al., 2002, 2004; Waugh et al., 2006) with most of the stored C_{anth} found in the shallowest ~1,500 m of the Pacific basin, the lowest reaches of which are ventilated by Antarctic Intermediate Water, Subantarctic Mode Water, and other thermocline water masses such as North Pacific Intermediate Water.

Repeat hydrographic surveys allow C_{anth} accumulation rates to be quantified from changes in observed dissolved inorganic carbon (DIC) distributions and the assumption that other processes governing DIC variability have consistent or predictable impacts on seawater properties. This approach has been used to update 1990s era estimates of Pacific C_{anth} (Sabine et al., 2004) for a range of decades (Carter, Feely, Mecking, et al., 2017; Chu et al., 2016; Kouketsu et al., 2013; Kouketsu & Murata, 2014; McNeil et al., 2001; Murata et al., 2007; Peng et al., 2003; Sabine et al., 2008; Wakita et al., 2010; Waters et al., 2011; Williams et al., 2015). One of the most widely applied approaches for estimating decadal C_{anth} changes from repeated hydrographic measurements is the Multiple Linear Regression (MLR) approach (Wallace, 1995). The method uses empirical linear relations between observed seawater properties (e.g., temperature T or potential temperature θ, salinity S, oxygen concentration O_2 or apparent oxygen utilization AOU, total titration seawater alkalinity A_T, nitrate N, silicic acid Si, and phosphate P) and DIC concentrations in the same samples to capture the influences of natural variability (e.g., interior ocean mixing, isopycnal heave, movements of fronts and eddies, and cycling of organic matter and carbonate minerals) on DIC distributions. The regressions from one set of observations are then applied to property distributions from another year to yield an estimate of the DIC distributions that would be expected had the various modes of change acted identically in both years. In the simplest implementation of the MLR approach, the differences between the observed and reconstructed DIC distributions are then attributed to C_{anth} accumulation (e.g., Sabine et al., 1999). The method therefore relies on the assumption that C_{anth} accumulation is uncorrelated with the impacts of long-term trends in the other seawater properties (Plancherel et al., 2013; Wallace, 1995).

Here, we summarize and combine several modifications that have been proposed for the MLR approach, assess the combined methods (supporting information S1) and apply the updated method to 14 sections in the Pacific Ocean and in the Pacific sector of the Southern Ocean (Figure 1). Finally, we develop an approach by which C_{anth} accumulation can be estimated in regions not located directly along these specific sections. We produce results consistent with Gruber, Clement, et al. (2019)'s recent finding that the Pacific took up 39

(±4)% of a global 34 (±4)-PgC accumulation from 1994 to 2007 and also extend the Pacific accumulation estimates through 2015. The newest section repeats build on the initial global survey conducted under the World Ocean Circulation Experiment and the Joint Global Ocean Flux Study in the late 1980s and early 1990s (Wallace, 2001) and are measured as part of the global repeat hydrography effort now sustained by the Global Ocean Hydrographic Investigations Program (GO-SHIP; Talley et al., 2016).

Now having three nearly complete decades worth of measurements along Pacific repeat hydrographic lines affords a comparison of our results to those of recent studies exploring interannual variability in carbon cycling. Li and Ilyina (2018) indicated that the ocean DIC accumulation rate should accelerate over time while also experiencing significant decadal variability. This is consistent with recent findings (e.g., DeVries et al., 2017; Gruber, Clement, et al., 2019; Gruber, Landschützer, et al., 2019; Landschützer et al., 2016). Specifically, Landschützer et al. (2016) show that a significant slowdown occurred in the ocean uptake of CO_2 relative to expectations from atmospheric CO_2 accumulation between ~1994 and ~2008 and that this change predominantly originated in the Southern Ocean (defined broadly as the ocean south of 35°S). DeVries et al. (2017) accounted for the recent ocean CO_2 rebound by arguing that a slowdown in overturning circulation elevated retention of natural CO_2 in the Southern Hemisphere between 2000 and 2010 by more than it slowed C_{anth} uptake. However, they note their methods do not resolve circulation-induced changes in nutrient supplies to the surface ocean that could—by modulating the soft tissue pump—dampen natural air-sea flux CO_2 variability. Our analysis adds to this discussion by directly comparing the 1995 to 2005 period to the period from 2005 to 2015, which means that our estimates for the earlier period correspond closely to the anomalously low total CO_2 flux periods identified by Landschützer et al. (2016), as well as to the C_{anth} accumulation estimates of Gruber, Clement, et al. (2019). Our study is the first analysis that examines Pacific decadal C_{anth} variability based on direct comparisons of ocean interior carbon measurements over three decades along more than two sections. We argue that C_{anth} accumulation variability can explain much of the total (i.e., natural and anthropogenic) CO_2 air-sea exchange variability, and suggest that there was a meaningful circulation-induced increase in Pacific Ocean C_{anth} accumulation starting late in the 2000 to 2010 decade that was not yet reflected in the data product (Olsen et al., 2016) that DeVries et al. (2017)'s model assimilated.

2. Methods

2.1. Evolution of the MLR Approach

Many modifications to the MLR approach have been proposed to address various shortcomings of the method: Friis et al. (2005) showed that misfits between the empirical regressions of DIC and the measured DIC distributions could lead to large regional biases when interpreted directly and articulated the "extended" MLR (eMLR) method, which estimates C_{anth} changes as residuals between two sets of regressions fitted to two repeat sections separately when applied to a single distribution of properties (as was done earlier by Wallace, 1995). To a degree, the fit biases tend to cancel with this approach, with the added benefit that eMLR greatly limits the impact of random measurement errors (Clement & Gruber, 2018). However, it does little to remedy the impacts of systematic measurement biases (Carter, Feely, Mecking, et al., 2017). Quay et al. (2007) found that residuals for the MLR fits could be improved if separate fits were created for data binned by density intervals. Goodkin et al. (2011) cautioned that over >30-year time periods the assumption that the same modes of natural variability are acting on water at a given location may break down. Plancherel et al. (2013) showed that reconstruction errors are smaller and less biased on average when using data from sections with consistent station locations. They argue that consistent sampling ensures that the MLR models are fit to the same oceanographic features, therefore increasing the chances that the models will be biased consistently between decades, allowing the biases to cancel. They also show that the C_{anth} change estimates yielded by eMLR are dependent upon the choice of the independent variables used to construct the empirical regressions.

More recently, Carter, Feely, Mecking, et al. (2017) used averages of an ensemble of C_{anth} distribution estimates obtained from regressions fit to multiple different combinations of independent variables. Their ensemble approach decreased both bias and root-mean-squared (RMS) error when reconstructing Earth System Model simulation output with known C_{anth} distributions. Clement and Gruber (2018) showed that an ensemble average limited to the regressions with the lowest root-mean-squared error (RMSE) of the regression fit to the DIC was better than a full-ensemble average for basin-sized layers. They also argued that C* (Gruber et al., 1996) is superior to DIC as the independent variable when making eMLR-based estimates because C* has some of the influences of natural variability removed. However, our analysis indicates that measurement biases should be considered when using this approach on individual sections (supporting information S1).

Thacker (2012) noted that it is unlikely that a single occupation could capture the full range of natural variability affecting seawater DIC distributions and demonstrated improvements by including both the earlier and the later occupations in the fitting data for a single combined regression. The C_{anth} accumulation rate from Thacker (2012)'s approach comes via inclusion of "occupation year" in the MLR for DIC. The accumulation rate estimate then equals the regression coefficient for occupation time. This approach has the drawback that the rate obtained from this approach is constant for an entire regression region, so Thacker (2012) advocated only considering limited subsets of a section with each regression.

2.2. Method Overview

In this study we combine recent methodological improvements by merging multiyear regressions (Thacker, 2012) with ensemble MLR (Carter, Feely, Mecking, et al., 2017), applying Velo et al. (2013)'s "moving (spatial) windows" to the data included in the regressions, using adjusted-DIC (Clement & Gruber, 2018) and using a weighted average of ensemble members. With the moving window approach, regressions are performed specific to a point in space using data selected within windows of latitude, longitude, and depth/density around that point in space. The regressions therefore adjust, spatially, to different combinations of data local to the intended regression location. Use of moving windows addresses Thacker (2012)'s suggestion that limited subsets of sections be considered at a time when using multiyear regressions (Carter, Feely, Mecking, et al., 2017). Thacker (2012)'s multiyear regression approach has a practical advantage compared to other eMLR approaches (e.g., Carter, Feely, Mecking, et al., 2017; Clement & Gruber, 2018) in that it accommodates data from hydrographic sections with three or more occupations, sometimes separated only by short periods of time (e.g., the SR03 section with measurements in 1995, 1996, 2008, and 2011), obviating the need for adjustments of data to a given reference year. Although this modified approach could miss C_{anth} variability at scales smaller than the moving window for data selection, our testing with model output indicated that Thacker (2012)'s approach nevertheless has a 4% smaller RMS error than the eMLR approach when reconstructing known modeled C_{anth} changes from model simulation output with added measurement uncertainties (supporting information S1).

Our modified approach combining these improvements is referred to here as the "$\underline{C}_{anth}$ $\underline{a}$ccumulation $\underline{r}$ates $\underline{e}$stimated from $\underline{e}$nsembles of $\underline{r}$egressions" (CAREER) approach. The errors for the approach are assessed for individual estimates and basin inventories, alongside the errors for individual estimates from similar approaches, in supporting information S1. An overview and a stepwise description of the technique is provided as supporting information S2.

2.3. Data Selection and Regressions Used

Measurements of S, θ, AOU, N, Si, DIC, and A_T are taken from version 2 of the Global Data Analysis Project (GLODAPv2) data product whenever possible (Olsen et al., 2016). These data include the GLODAPv2 adjustments based on deep crossovers between sections (https://glodapv2.geomar.de/). Recent (i.e., after ~2012) data that are not part of GLODAPv2 are downloaded from the Carbon and CLIVAR Hydrographic Data Office website (https://cchdo.ucsd.edu or https://www.nodc.noaa.gov/ocads/). A complete list of sections, Expocodes, PIs, cruise dates, 2,500 to 4,000-m average linear (S, θ, DIC, and A_T), and multiplicative (N, Si, and P) property offsets between each successive cruise pair and quality control notes are provided as supporting information S4 (CruiseInformation.xlsx). The offsets presented therein are separate from the GLODAPv2 adjustments and were used only to decide which data to include. No adjustments were made to the data other than the GLODAPv2 recommended adjustments.

Plancherel et al. (2013) noted that it is important to use consistent sampling locations for all occupations of a section. We thus removed data from consideration if they are located more than 120 nautical miles (nm) from a station measured along another occupation of the same section. This criterion is relaxed to 300 nm for the "West Coast Ocean Acidification" WCOA section, which had uneven station spacing over the same broad area in two complete reoccupations. In addition, data are omitted if they exceed the zonal or meridional limits of the cruise occupation with the shortest zonal (for zonal sections) or meridional (for meridional

10.1029/2018GB006154

sections) extents. The WCOA cruises were treated as meridional cruises (Figure 1). The number of stations omitted for each cruise is also given in supporting information S4.

In the CAREER approach, regressions are specific to individual data point locations in the second cruise along each section, and for each measurement on that second cruise, data are included in the regression if they are measured along the same section (from any year) and within latitude, longitude, and depth/density windows centered on the regression location. The initial sizes of the windows around the regression coordinates are 10° latitude, 20° longitude divided by the cosine of the latitude, and the union of both a 50-m depth and a 0.1-kg/m^3 σ_θ potential density vertical window. The window dimensions are iteratively doubled in size if fewer than 50 data points fall within the windows until at least 50 data points with viable C^ values are selected for the regression, where C^ is a simplified variant on C* (Gruber et al., 1996) defined here as

$$C^{=}DIC - r_{C:O2}O_2 \tag{1}$$

The $r_{C:O2}$ term (equaling −117/170 mol C mol O_2^{-1}; Anderson & Sarmiento, 1994) reflects the impact of organic matter remineralization on DIC (sensitivity to this assumed value is tested in supporting information S1). Unlike Clement and Gruber (2018) we do not include adjustments for carbonate mineral cycling nor do we use A_T as a predictor because our analysis indicated that increases in uncertainty resulting from measurement biases in the required parameters outweigh the potential benefits from these adjustments, at least when considering sections individually (supporting information S1). For similar reasons we also do not include adjustments for denitrification like Sabine et al. (2002).

The regressions relate C^ to 16 combinations (supporting information Table S3) with *n* predictor properties

$$C^{=}\alpha_0 + \sum_{i=1}^{n} \alpha_i P_i \tag{2}$$

Here α_i is the regression coefficient for the *i*th property (P_i) included in the regression and α_0 is a constant. Regression coefficients are determined through least squares "robust regression" that iteratively tests for and then excludes outlier data (where outliers are more than 4.685 deviations from the regression by default, though we get similar results without applying this best practice exclusion step). Phosphate is not used in these regressions because it provides little additional statistical information not provided by *N* and AOU (Slansky, 1997), and the phosphate measurement uncertainty is relatively larger than the nitrate uncertainty. Decimal year *Y* (i.e., where 1 July 2020 is "2020.5") is included in every regression (Thacker, 2012).

We excluded data from shallower than 50 m or the deepest monthly mean mixed layer depth in the climatology of Holte et al. (2017), whichever was deeper. Shallower than these depths, C_{anth} was determined assuming the full equilibration of seawater changes with the atmospheric mole fraction of CO_2 (xCO_2) increases as recorded at Cape Grim (the rationale for using Cape Grim is given in supporting information S3, but we note that this choice has little impact on our results). The simplistic assumption of tracking atmospheric changes is used because near-surface waters are strongly impacted by seasonal, subseasonal, and shorter-timescale processes that make the eMLR approach less viable (Sabine et al., 1999). Including near-surface data would both yield poor surface estimates and also potentially bias deeper regression coefficients. While there is substantial natural variability in surface partial pressure of CO_2 (pCO_2) mooring record trends (Sutton et al., 2017), the longer-term global mean surface ocean pCO_2 increase is broadly consistent with anthropogenic forcing (Bates et al., 2014; Landschützer et al., 2016) indicating that the surface change assumption is a plausible simplification for the surface anthropogenic component.

CO2SYS for Matlab (van Hueven et al., 2011) is used to calculate the impacts of changes in pCO_2 (and later C_{anth}) using the carbonate coefficients from Lueker et al. (2000) and the total hydrogen ion pH scale. For consistency, borate coefficients from Uppström (1974) are used instead of the updated coefficients determined by Lee et al. (2010) because the earlier coefficients were used by Lueker et al. (2000) and are thus consistent with their coefficients (see: Orr et al., 2015). The mixed layer calculations are performed at 0-dbar pressure and using the potential temperature (relative to 0-dbar pressure) to determine air-sea equilibration. In situ conditions are used for all other carbonate system calculations to quantify the impacts of C_{anth} on pH and aragonite saturation state (Ω) where C_{anth} is found. Where surface A_T is not measured, it is estimated from S, θ, and AOU using Locally Interpolated A_T Regression (equation 7; Carter, Feely, Williams, et al., 2017). Uncertainties in these calculations are dominated by errors in the assumed pCO_2 or DIC property changes and are relatively insensitive to uncertainties in the estimated A_T.

After the regressions are completed, the regression terms associated with the years (i.e., the 16 α_Y terms) are averaged—weighted using the inverse of the α_Y coefficient uncertainties—to obtain CAREER C_{anth} accumulation rate estimates (R_{Canth}) for the period spanned by all data along each section. $N - 1$, where N is the number of occupations of each section; accumulation rate estimates between one occupation of a section and the next occupation are also computed excluding all other data from that section besides the two occupations being compared. We refer to estimates using all data as "full-record rate estimates" and estimates using only one time interval, two section occupations at a time, as "successive-occupation rate estimates." For sections with only two viable occupations (e.g., P13, P14, and P21) the full-record and successive-occupation rate estimates are identical.

2.4. Extending C_{anth} Accumulation Rates to Total C_{anth}

Total C_{anth} is estimated by referencing our accumulation rate estimates to Sabine et al. (2004)'s ΔC*-based C_{anth} 1994 distribution, as gridded by Key et al. (2004), interpolated by potential density to our measurement densities (see supporting information S1 for details). For each section, we begin with the earliest "successive-occupation" accumulation rate estimates and use these to project backward in time from 1994 and forward in time to the date of the second occupation. The next set of C_{anth} accumulation rate estimates is then used to project forward until the year of the next cruise occupation (if any exists). The procedure by which we interpolate C_{anth} along sections from one occupation to the next is provided in supporting information S2.

Tracking the impacts of C_{anth} on ocean pH is an important application for C_{anth} estimates, as it allows inferences about the degree to which organism habitats have been perturbed from their natural states. Once total C_{anth} estimates are obtained, "preindustrial" in situ pH and Ω are estimated for each decade by subtracting the C_{anth} estimates along each occupation from the DIC observed during the same occupation and recalculating the pH and Ω. The impacts of ocean acidification on pH and Ω (ΔpH and ΔΩ, respectively) are then calculated as the preindustrial values subtracted from the modern calculated values.

A new method, related to the multiparametric interpolation of Velo et al. (2010), is used to extrapolate the total C_{anth} estimates to the basin scale. A locally interpolated regression (LIR) (Carter, Feely, Williams, et al., 2017) is created relating C_{anth} to S, θ, the depth, the years since 1995 (Y_{1995}, with a maximum of 10), and the years since 2005 (Y_{2005}, with a minimum of 0). As the LIR is used solely for basin-wide estimation, we only briefly note that the methods of its creation in all ways mirror those of Locally Interpolated A_T Regression version 2 as presented by (Carter, Feely, Williams, et al., 2017), with the following exceptions: (1) Only a single regression is used. (2) Data incorporation windows are set to 30° latitude and 60° longitude. These are necessarily larger than the windows used for CAREER estimates because these regressions are not always centered on repeated hydrographic sections where nearby data are guaranteed, and data are needed for at least three distinct dates to fit both Y terms. (3) To ensure the regressions remain "local" to the extent possible, the training data are weighted according to the inverse of three distance terms added in quadrature. The weighting term W is calculated separately for each combination of properties and C_{anth} estimate being regressed

$$W = \max\left(20, \left((4(\mathrm{Lat_m} - \mathrm{Lat_r}))^2 + (\cos(\mathrm{Lat_r})(\mathrm{Lon_m} - \mathrm{Lon_r}))^2 + \left(\frac{\mathrm{depth_m} - \mathrm{depth_r}}{100\ \mathrm{meters}}\right)^2\right)^{-0.5} \quad (3)$$

Here Lat is the latitude, Lon is the longitude, "depth" is in meters, the subscript r refers to the coordinate of the regression, and the subscript m refers to the coordinate of the measurement being weighted. The factors of 4 and 1/100 meters reflect observations that ocean properties typically vary more meridionally and (especially) vertically than zonally. Weights are capped at $20^{-0.5}$ (or ~0.224) to avoid the nearly infinite weights that would otherwise occur at grid cells adjacent to or on hydrographic sections, ensuring that a number of values affect the regressions.

The LIR allows a local C_{anth} estimate to be obtained anywhere in the Pacific Ocean and Pacific sectors of the Southern Ocean from latitude, longitude, depth, S, T or θ, and Y (which the routine then uses to calculate Y_{1995} and Y_{2005}). The LIR reproduces the training data (total C_{anth} estimates in the years the sections were measured, i.e., including no temporally interpolated or extrapolated data) well with errors of −0.022 (average) ±2.6 (RMSE) μmol kg^{-1} C_{anth}. To estimate likely errors encountered in parts of the Pacific where C_{anth} estimates are unavailable, each CAREER estimate was reconstructed using a LIR that is trained separately at each of the C_{anth} estimate locations but excluding the C_{anth} estimates from occupations of the section that produced the estimate being tested. This experiment suggested slightly larger reconstruction errors of 0.038 (average) ±3.5 (RMSE) μmol kg^{-1} C_{anth}.

The LIR is applied to the World Ocean Atlas annual average data product (Locarnini et al., 2013; Zweng et al., 2013) with Y inputs of 1995, 2005, and 2015, and these estimates are multiplied by calculated in situ densities and the grid cell ocean volumes and summed over the top 1,500 m to yield basin C_{anth} inventory estimates. Uncertainties in basin inventories for these 3 years are dominated by potential errors in the 1994 reference ΔC*-based C_{anth} distributions (±5 μmol kg^{-1} basin-wide C_{anth}). However, these errors should be consistent between decadal estimates and therefore cancel when computing decadal basin inventory changes. This suggests that the majority of the uncertainty for decadal basin inventory changes is attributable to CAREER estimate errors (i.e., section-wide biases of ±1.4 μmol kg^{-1} C_{anth}, which only partially cancel for basin averages; supporting information S1).

3. Results and Discussion

3.1. Full Record Accumulation Rates

C_{anth} accumulation rates typically range from ~0 μmol·kg^{-1}·$year^{-1}$ at depth (>1,500 m) to ~1.1 μmol·kg^{-1}·$year^{-1}$ in the warmer regions of the surface ocean. The C_{anth} accumulation rates (Figure 2) agree with earlier C_{anth} accumulation estimate patterns from observations and models (e.g., Carter, Feely, Mecking, et al., 2017; Kouketsu et al., 2013; Waters et al., 2011), as expected from air-sea CO_2 exchange patterns and interior ocean transport (Talley et al., 2016, and references therein): Pacific C_{anth} accumulation rates are greatest in shallow thermocline waters with the lowest potential densities (σ_θ), both because these waters are well ventilated and because warmer surface waters with little remineralized DIC typically have lower Revelle Factors (Revelle, 1934) and therefore exhibit a larger DIC increase in equilibrium with a given anthropogenic pCO_2 increase.

Pacific C_{anth} accumulation and storage patterns do not geographically match C_{anth} uptake patterns (e.g., Gloor et al., 2003; Sarmiento et al., 1992). The discrepancy between the patterns of uptake and accumulation is due largely to interior ocean transport of C_{anth} from the high-latitude regions where C_{anth} is primarily taken up from the atmosphere to the midlatitude thermoclines where it is primarily stored (e.g., Mikaloff Fletcher et al., 2006). The P16 section near 150°W captures most of the meridional gradients in C_{anth} accumulation seen across the basin (Figure 2a): There is substantial accumulation in the surface ocean ranging from >1.1 μmol·kg^{-1}·$year^{-1}$ in the warm equatorial latitudes to ~0.7 μmol·kg^{-1}·$year^{-1}$ at higher latitudes and deeper penetration (up to ~1,500 m) of C_{anth} in the subtropical gyres. The penetration is deeper particularly in the subtropics of the Southern Hemisphere where Subantarctic Mode Water and Antarctic Intermediate Water ventilate to the base of the subtropical gyre (Sabine et al., 2008; e.g., 0.3 vs. 0.0 μmol·kg^{-1}·$year^{-1}$ at 900-m depth along 40°S vs. 40°N, respectively). C_{anth} accumulation is shallower near the equator and within the divergent subpolar gyres. These Southern Hemisphere and equatorial C_{anth} accumulation patterns are also seen along P15, P18, and SR03 (Figures 2b, 2c, and 2g), while the Northern Hemisphere and equatorial features are seen along P10, P13, and P14 (Figures 2d–f). The zonal C_{anth} accumulation rate sections indicate deeper C_{anth} accumulation on the poleward and central portions of the subtropical gyres (Figure 3d) than equatorward (Figure 3c) and deeper accumulation in the convergence areas of the subtropical gyres than in the divergent subpolar gyres (Figure 3). Zonally, Pacific C_{anth} accumulation tends to accumulate deeper near the western edges of the subtropical gyres (Waters et al., 2011). This is visible for the P02 (Figure 3b), P21 (Figure 3c), and P06 (Figure 3d) sections where C_{anth} accumulation rate isopleths shoal to the east.

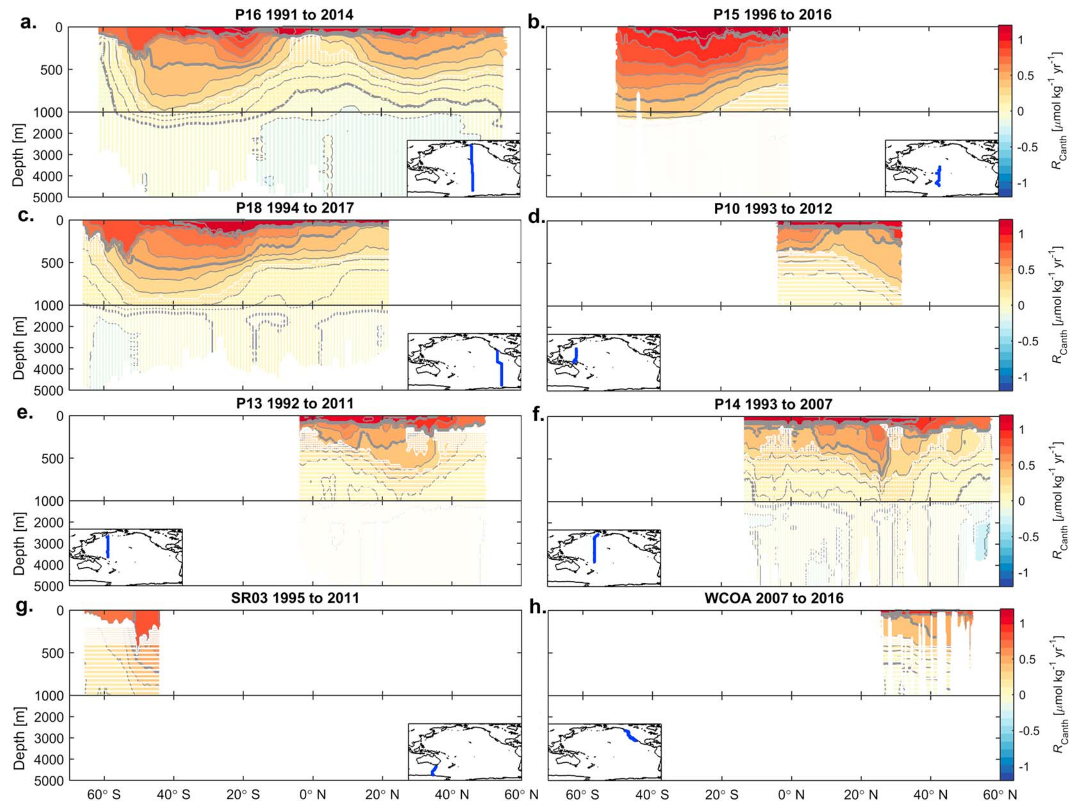

Figure 2. C_{anth} accumulation rates estimated for the predominantly meridional sections (a) P16 along ~150°W, (b) P15 along ~170°W, (c) P18 along ~103°W to 110°W, (d) P10 along ~140°E to 150°E, (e) P13 along ~165°E, (f) P14 along ~175°W to 180°W, (g) SR03 along ~140°W to 150°W, and (h) WCOA along a series of section extending from the U.S. West Coast (see Figure 1). Time spans of these estimates are given in the panel titles. Estimates with colors covered by white dots are not statistically distinguishable from 0 change to greater than 95% confidence. Thick gray contours demark every 0.5 μmol/kg beginning at 0, and thinner gray contours demark every 0.1 μmol/kg. Inset maps indicate the section locations. WCOA = West Coast Ocean Acidification.

Along the zonal S04I (Figure 3e) section (~60–65°S) a small but significant C_{anth} signal extends along the ocean floor (averaging 0.24 μmol·kg^{-1}·year^{-1} below 1,500 m and east of 120°E) where Katsumata et al. (2015) previously reported near-bottom warming, freshening, and AOU decreases and where Murata et al. (2019) detected significant increases of anthropogenic CO_2 in deep and bottom layers. Deep ocean C_{anth} accumulation is also present along the intersecting meridional SR03 section (Figure 2g), although this moderate signal is not statistically distinguishable from zero at these depths and latitudes in our estimates or in prior analyses (Pardo et al., 2017). Sabine et al. (2002) reported measurable chlorofluorocarbons (CFCs) and therefore estimated small concentrations of C_{anth} at depths >2,000 m along both sections. These two sections provide further evidence that Antarctic Bottom Water, which is known to be warming and freshening over large regions (Purkey & Johnson, 2013), is also bringing C_{anth} into the deep Southern Ocean on decadal timescales (as Ríos et al., 2012, reported in the Atlantic). These signals go from the surface to the ocean floor and extend slightly off the continental shelf, though blurring—from the wide windows required for the CAREER analysis— is possible of a narrower accumulation along the continental margin that might be expected from entrainment of C_{anth} into Antarctic Bottom Water. Abyssal accumulation is also positive but not independently statistically significant along the western portion of S04P. The lower accumulation estimates below the center of the Ross Sea Gyre than further west are consistent with pathways of Adélie Land Bottom Water formed east of SR03 (Rintoul, 1998) and Ross Sea Bottom Water brought north in a deep western boundary current past Cape Adare (Gordon et al., 2015). Consistent with these C_{anth} estimate patterns, significant deep C_{anth} (Sabine et al., 2002) and CFC (Orsi et al., 1999) concentrations have been observed on the eastern and northern boundaries of the Ross Sea that do not extend to the S04P transect through the center of the Ross Sea.

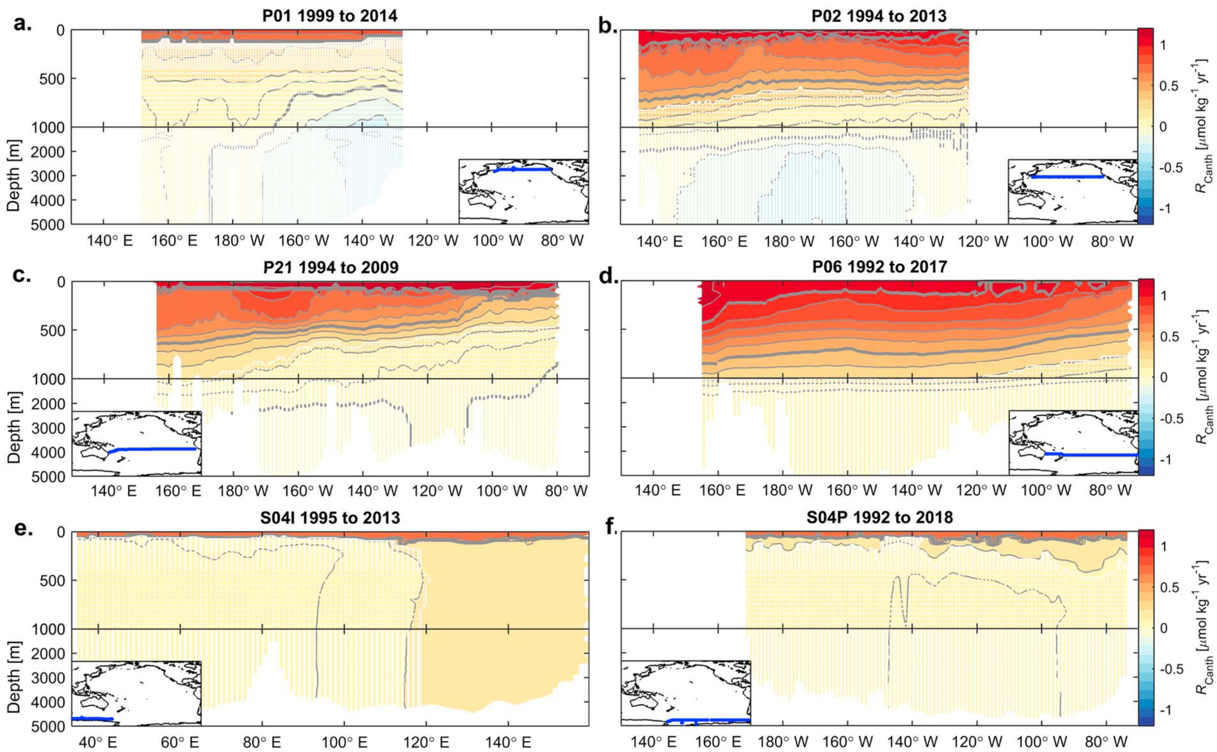

Figure 3. C_{anth} accumulation rates estimated for the zonal (east-west) sections (a) P01 along 40°N to 47°N, (b) P02 along 30°N to 33°N, (c) P21 along 15°S to 25°S, (d) P06 along 30°S to 33°S, (e) S04I along 43°S to 67°S, and (f) S04P along 65°S to 71°S (mapped in Figure 1). Time spans of these estimates are given in the panel titles. Estimates with colors covered by white dots are not statistically distinguishable from 0 change to greater than 95% confidence. Thick gray contours demark every 0.5 μmol/kg beginning at 0, and thinner gray contours demark every 0.1 μmol/kg. Inset maps indicate the section locations.

3.2. Column C_{anth} Inventory Increases

We consider column inventory changes along sections down to 1,100 m. This is shallower than the integration depth used for the basin inventory estimates (presented in the next section) because those benefit from potentially canceling measurement biases along the 14 sections used to create them whereas section inventory estimates do not. Thus, the signal-to-noise ratio is lower for column inventory estimates and the depth at which observed changes are likely to be spurious is shallower.

Column inventory increases over the top 1,100 m of the Pacific along meridional (Figure 4) and zonal (Figure 5) sections match the accumulation rate estimates, with larger C_{anth} inventory increases in the subtropics than near the poles or at the equator (e.g., Figure 4a) and larger increases in the western portions of the gyres (e.g., Figures 5c and 5d) than in an eastern boundary current (Figure 4g). However, column inventory increases also show considerable variability from decade to decade (Figures 4 and 5, comparing color-shaded regions), notably including the larger column inventory increases in the recent decades along the equatorward sides of the Southern Hemisphere Subtropical Gyre (Figures 4a–4c). Carter, Feely, Mecking, et al. (2017) reported C_{anth} column inventory increased along P16 at a rate of 0.29 (±0.11) mol C·m^{-2}·year^{-1} from 1991 to 2005 and at a rate of 0.45 (±0.11) mol C·m^{-2}·year^{-1} from 2005 to 2015. We find comparable rates of 0.31 (±0.13) and 0.43 (±0.20) mol C·m^{-2}·year^{-1} for these two periods, respectively (Table 1).

Interdecadal variability in C_{anth} inventory increases are attributable to decadal change in C_{anth} uptake and transport to an extent, but the large uncertainty intervals imply that there is a limit on the accuracy of C_{anth} accumulation estimates along a single section from a single decade. The majority of column inventory uncertainty is attributable to the potential for unknown biases in the measurements: consider that the ±1.4 μmol kg^{-1} estimate bias translates to ±1.6 mol C m^{-2} when summed over 1,100 m or 0.16 mol C·m^{-2}·year^{-1} after a decade. At least ~60% of this bias is attributable to measurement biases instead of methodological errors (supporting information S1). The relative impacts of measurement errors on C_{anth} accumulation rates decrease over time and with repeated occupations, both due to more independent and partially canceling

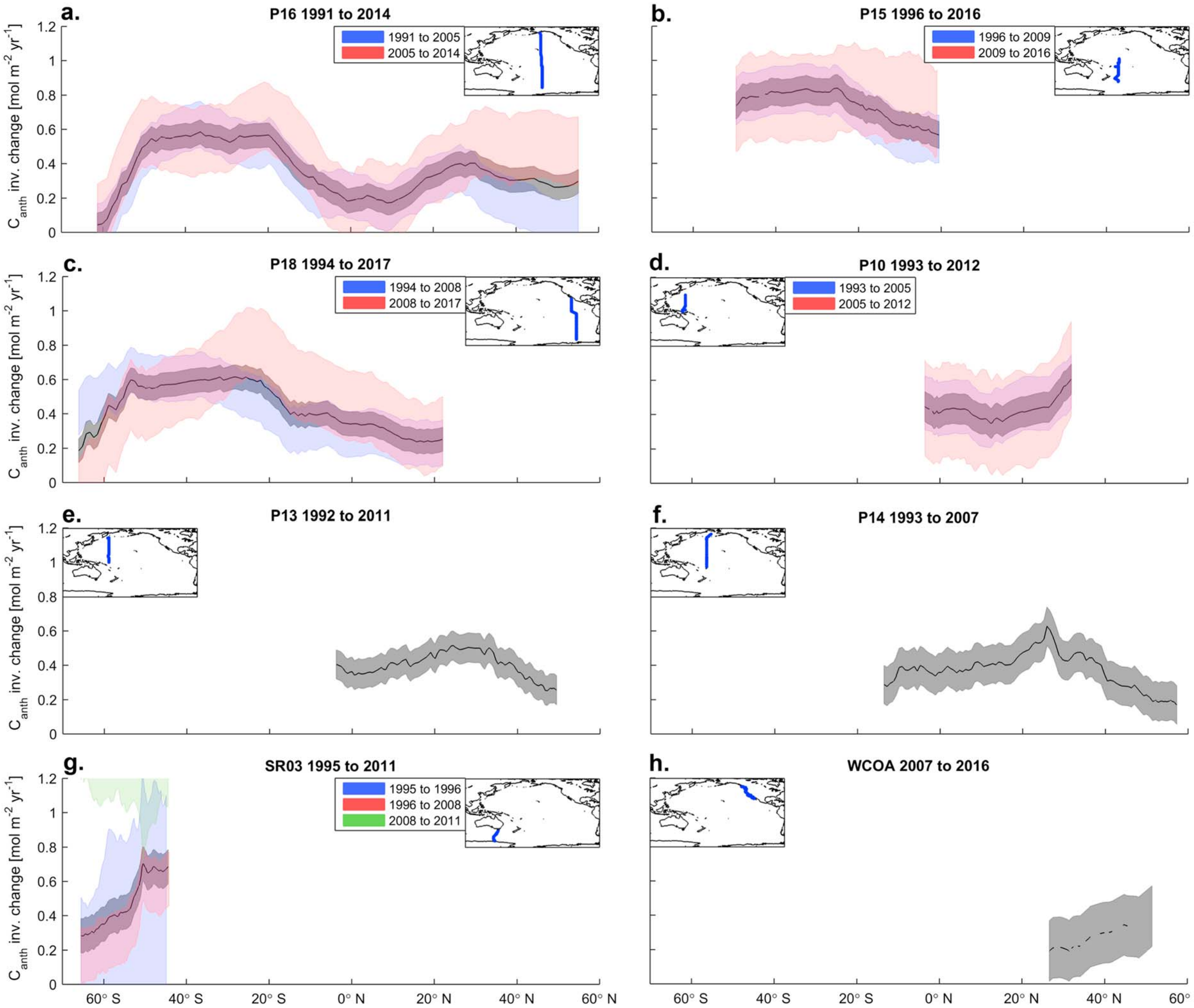

Figure 4. C_{anth} accumulation rates expressed as column inventories over the top 1,500 m of the water column along meridional sections (a) P16 along ~150°W, (b) P15 along ~170°W, (c) P18 along ~103°W to 110°W, (d) P10 along ~140°E to 150°E, (e) P13 along ~165°E, (f) P14 along ~175°W to 180°W, (g) SR03 along ~140°W to 150°W, and (h) WCOA along a series of section extending from the U.S. West Coast (see Figure 1). Estimates (black lines, broken where shallow waters prevented a full 1,500-m integral) are shown with uncertainties (red, blue, and gray bands). Time spans of these estimates are given in the panel titles (and the figure legends when multiple estimates are available). Inset maps indicate the section locations. WCOA = West Coast Ocean Acidification.

measurement biases and larger signal accumulating over a longer time span. The decreasing error bounds in column inventory changes along P06 (Figure 5d), for example, demonstrate the substantial improvements in signal/noise obtained with long-term records. Combining information from several repeated hydrographic sections (as we do in the next section and as Clement & Gruber, 2018, advocate) also reduces the inventory change uncertainties.

Numerous Pacific column inventory change estimates have been made previously (Table 1). Our estimates agree within 1σ (ours or theirs) with most of these estimates, though ours are lower than Sabine et al. (2008)'s north of 20°N (only) and Wakita et al. (2010)'s in the Northwest Pacific. These differences stem from our use of the recently released GLODAPv2 data product (Olsen et al., 2016) and the methodological improvements in the CAREER approach (supporting information S1). Our analysis indicates that errors from traditional eMLR approaches are ~20% greater than from CAREER when applied to the same sections, though earlier error estimates did not always consider parameter choice uncertainties so this may not be clear from Table 1.

3.3. Total Basin-Wide Inventories

We reference to the 1994 ΔC^*-based estimates of Sabine et al. (2004) to provide estimates of Pacific basin C_{anth} inventories summed to 1,500-m depth of 42.2 (±5), 50.9 (±5), and 62.6 (±5) PgC for 1995, 2005, and

10.1029/2018GB006154

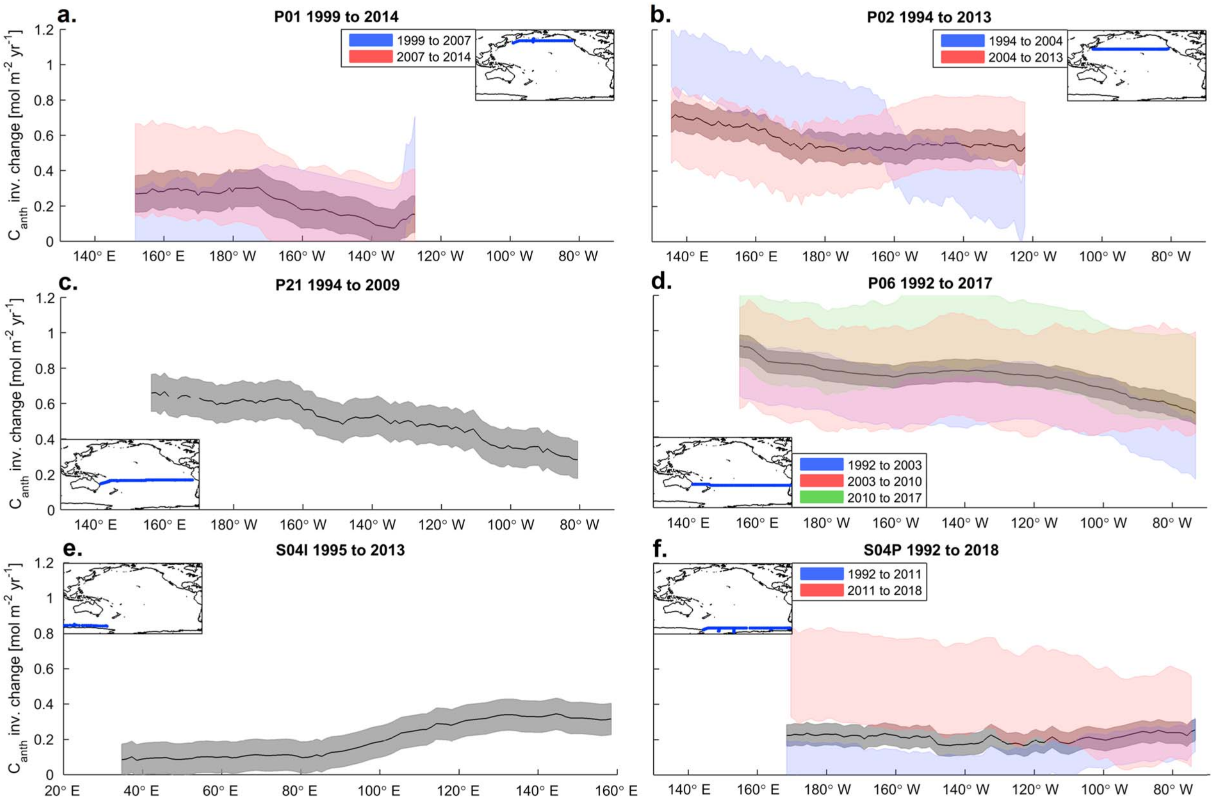

Figure 5. C_{anth} accumulation rates expressed as column inventories over the top 1,500 m of the water column along zonal (east-west) sections (a) P01 along 40°N to 47°N, (b) P02 along 30°N to 33°N, (c) P21 along 15°S to 25°S, (d) P06 along 30°S to 33°S, (e) S04I along 43°S to 67°S, and (f) S04P along 65°S to 71°S (mapped in Figure 1). Estimate (black lines, broken where ocean depths prevented a full 1,500-m integral) and uncertainties (blue, red, green, and gray bands) are shown. Time spans of these estimates are given in the panel titles and legends.

Table 1
Column Inventory (Top 1,100 m) Increases Compared to a Compilation of Literature Estimates

Study	Section	Method	Their rate σ±	Our rate σ±	Time Span
			[mol m^{-2} yr^{-1}]	*[mol m^{-2} yr^{-1}]*	
Murata et al. (2007)	P06	ΔnC_T^{Cal}	1.0 ± 0.4	0.62 ± 0.16	1992–2003
Sabine et al. (2008)	P16 N of 20°N	eMLR	0.4 ± 0.1	0.20 ± 0.13	1991–2006
Sabine et al. (2008)	P16 20°S to 20°N	eMLR	0.3 ± 0.1	0.26 ± 0.13	1991–2006
Sabine et al. (2008)	P16 60°S to 20°S	eMLR	0.6 ± 0.1	0.48 ± 0.13	1991–2006
Sabine et al. (2008)	P16 S of 60°S	eMLR	0.1 ± 0.1	0.04 ± 0.13	1991–2006
Murata et al. (2009)	P10	ΔnC_T^{Cal}	0.5 ± 0.1	0.45 ± 0.16	1993–2005
Wakita et al. (2010)	~160°E to 45°N	DIC with ΔC*	0.4 ± 0.1	0.29 ± 0.10	1992–2008
Waters et al. (2011)	P06	TTD	0.72 ± 0.2	0.74 ± 0.11	1992–2010[a]
Waters et al. (2011)	P06	eMLR	0.79 ± 0.2	0.74 ± 0.11	1992–2010[a]
Waters et al. (2011)	P18	eMLR	0.46 ± 0.2	0.32 ± 0.13	1994–2008
Williams et al. (2015)	S04P	eMLR	0.1 ± 0.02	0.09 ± 0.10	1992–2011
Pardo et al. (2017)	SR03	C_T^0	0.3 ± 0.24	0.31 ± 0.11	1995–2011
Carter, Feely, Mecking, et al. (2017)	P16	Ensemble eMLR	0.29 ± 0.11	0.31 ± 0.13	1991–2005
Carter, Feely, Mecking, et al. (2017)	P16	Ensemble eMLR	0.45 ± 0.11	0.43 ± 0.20	2005–2015
Carter, Feely, Mecking, et al. (2017)	P02	Ensemble eMLR	0.53 ±0.11	0.65 ± 0.17	1991–2004
Carter, Feely, Mecking, et al. (2017)	P02	Ensemble eMLR	0.46 ± 0.11	0.56 ± 0.21	2005–2013

[a]Our comparison estimate goes ~7 years longer than this period.

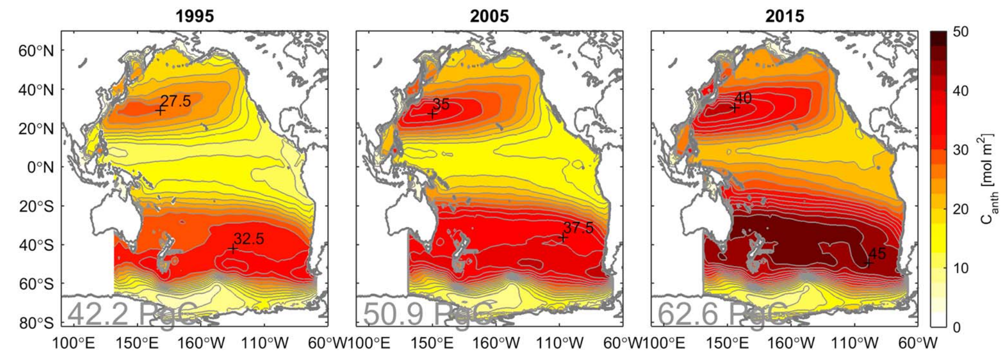

Figure 6. Column inventories contoured summed from the surface to 1,500-m depth in color for (left) 1995, (middle) 2005, and (right) 2015 in color and labeled in black. Thick gray contours demark every 10 mol/m^{-} beginning at 0, and thinner gray contours demark every 2.5 mol/m^2. The total Pacific Basin inventory is written in light gray. The inventories in the panel on the left are lower than the inventories they are based on (44.5 ± 5 PgC for 1994; Sabine et al., 2002), especially in the Southern Ocean, due primarily to the shallower depth of integration. Decadal changes of the zonal integrals of these inventories are provided in Table 2.

2015, respectively. The Pacific C_{anth} inventory increased by 8.8 (±1.1) PgC between 1995 and 2005 and by 11.7 (±1.1) PgC (Figure 6) between 2005 and 2015. These increases suggest an average increase of 0.94 (±0.11) PgC $year^{-1}$ over the 1994–2007 time period, which compares well with Gruber, Clement, et al. (2019) findings of an average Pacific accumulation of 0.97 PgC $year^{-1}$ (when using our Pacific basin bounds and integrated to 1,500-m depth).

Kouketsu et al. (2013) estimated Pacific C_{anth} increased by 8.4 (±0.5) PgC between 50°S and 65°N in the earlier decade (1995 to 2005), where we find 7.7 (±1.1) PgC accumulation (Table 2). The majority of this (statistically insignificant) discrepancy originates in the 20°S to 50°S latitude band where Murata et al. (2007)

Table 2
Pacific Inventory Increases by Latitude Band for Both Decades, Compared to Literature

Latitude from (°N)	to (°N)	Δ Inventory 1995–2005 PgC	Comparison 1995–2005 PgC	Δ Inventory 2005–2015 PgC	Comparison 2005–2015 PgC
Comparisons to Carter, Feely, Mecking, et al. (2017), ensemble eMLR					
−80	−70	0.05 (±0.02)	—	0.04 (±0.02)	—
−70	−60	0.27 (±0.09)	—	0.06 (±0.09)	—
−60	−50	0.60 (±0.13)	*0.56*	0.45 (±0.13)	*0.84*
−50	−40	0.96 (±0.14)	*0.90*	1.06 (±0.14)	*0.97*
−40	−30	1.05 (±0.14)	*0.96*	1.47 (±0.14)	*1.07*
−30	−20	0.98 (±0.14)	*0.65*	1.63 (±0.14)	*1.31*
−20	−10	0.83 (±0.15)	*0.35*	1.66 (±0.14)	*1.20*
−10	0	0.67 (±0.15)	*0.29*	1.38 (±0.15)	*0.72*
0	10	0.84 (±0.15)	*0.46*	1.18 (±0.15)	*0.56*
10	20	0.85 (±0.13)	*0.79*	0.84 (±0.13)	*0.52*
20	30	0.81 (±0.10)	*0.60*	0.74 (±0.10)	*0.64*
30	40	0.50 (±0.08)	*0.35*	0.60 (±0.08)	*0.53*
40	50	0.21 (±0.06)	*0.13*	0.36 (±0.06)	*0.35*
50	60	0.13 (±0.03)	*0.07*	0.22 (±0.03)	*0.21*
60	70	0.05 (±0.01)	—	0.04 (±0.01)	—
Comparisons to Kouketsu et al. (2013), ΔnC_T^{Cal}, 120°E to 131°E included and marginal seas omitted for this comparison					
40	65	0.3 (±0.19)	*0.3 ± 0.2*	0.6 (±0.19)	—
20	40	1.3 (±0.21)	*1.5 ± 0.2*	1.3 (±0.21)	—
−20	20	3.1 (±0.45)	*2.7 ± 0.4*	5.0 (±0.45)	—
−50	−20	3.0 (±0.31)	*3.9 ± 0.3*	4.2 (±0.31)	—
−50	65	7.7 (±0.93)	*8.4 ± 0.5*	11.0 (±0.93)	—
Entire Pacific		8.8 (±1.1)	—	11.7 (±1.1)	—

Note. The italicized numbers come from other studies included for comparison.

10.1029/2018GB006154

found more C_{anth} than we do along P06 (Table 1). These estimates were also used for Kouketsu et al. (2013)'s basin storage synthesis. Carter, Feely, Mecking, et al. (2017) inferred storage estimates of 6.1 (±1.5) and 8.8 (±2.2) PgC for the full Pacific basin in the earlier and more recent decades, respectively, from P16 alone. When considering basin changes divided by latitude bands (Table 2), the majority of the (statistically insignificant) increase in the current estimates relative to Carter, Feely, Mecking, et al. (2017) earlier estimates in the 2005 to 2015 decade is found in the Southern Pacific and equatorial latitudes (~40°S to 10°N), where the added information from many cruises (e.g., P10, P13, P14, P18, P15, and P21) improved estimates and reduced the estimate uncertainty by half.

3.4. Decadal C_{anth} Accumulation Variability

For the entire Pacific, we find that the accumulation rate accelerated by 2.9 (±1.6) PgC decade^{-2} from the earlier decade (between 1995 and 2005) to the more recent decade (between 2005 and 2015). This acceleration is, however, only marginally statistically significant ($p = 0.07$) due to the large uncertainties of these decadal differences. Most of this acceleration stems from the South Pacific, that is, the region between 40°S and the equator (Table 2). There, the estimated decadal acceleration of 2.6 (±0.6) PgC decade^{-2} is highly significant ($p < 0.01$), consistent with enhanced storage within the Southern Pacific Subtropical Gyre observed along P06, P18, P16, and P15 in the successive occupation sections (Figure 7, with successive occupation sections for other sections in supporting information Figure S2 and accumulation rate changes in supporting information Figure S3).

Since atmospheric CO_2 continued to rise between the two decades, an acceleration of the accumulation rate is expected (e.g., Mikaloff Fletcher et al., 2006). We estimate this expected acceleration using two methods detailed in supporting information S3; these methods are a fixed-circulation transport matrix estimate and an estimate based on transient steady state accumulation assumptions (see: Gruber, Clement, et al., 2019). They result in a combined estimate of a 1.4 (±0.4) PgC decade^{-2} expected acceleration for the whole Pacific basin and a 0.5 (±0.2) PgC decade^{-2} acceleration for the Southern Pacific Subtropical Gyre. Thus, only about half of the acceleration for the entire Pacific can be attributed to the increase in atmospheric CO_2 (1.4 (±0.4) versus 2.9 (±1.6) PgC decade^{-2}),while for the Southern Pacific Gyre this fraction is only about one fifth (0.5 (±0.2) versus 2.6 (±0.6) PgC decade^{-2}). In other words, the accumulation rate in the Southern Pacific Subtropical Gyre accelerated by a whopping 2.1 (±0.6) PgC decade^{-2} beyond the increase expected from the accumulation of atmospheric CO_2 alone ($p < 0.01$).

Carter, Feely, Mecking, et al. (2017) attributed the increase along P16 to an increase in the overturning (or “spin-up”) of the gyre subtropical cell (England et al., 2014; McPhaden & Zhang, 2004) from the mid-1990s through at least 2014 (Roemmich et al., 2007, 2016). The maximum observed increase in accumulation shifts southward going from west to east: it is found north of 20°S along P15, broadly between 30°S and 5°S along P16, and between 35°S and 20°S along P18. Similarly, along P06 near 30°S, the increase is most intense in the east near P18 and, later, in the central Pacific near P16 (Figures S3d and S3e). The pattern in space (and time along P06) is consistent with enhanced ventilation or circulation of South Pacific Tropical Water late in the 2000s decade that propagates north and west before remerging, in part, in the equatorial Pacific (Qu et al., 2013; 18°S to 18°N) where we see a 1.3 (±0.3) PgC decade^{-2} C_{anth} accumulation acceleration between decades.

It is not straightforward to contrast anomalies in the rate of accumulation of C_{anth} in the ocean's interior with changes in the air-sea CO_2 fluxes inferred from surface pCO_2 measurements. The comparison is not direct both because the surface CO_2 fluxes are combinations of natural and anthropogenic signals and because interior ocean mixing can lead to CO_2 accumulation far from uptake. It is nevertheless instructive to attempt such a comparison as it might provide indications about the importance of the contribution of the fluxes in C_{anth} to the total variability in the air-sea CO_2 fluxes (see also Gruber, Landschützer, et al., 2019). The rapid increase in the accumulation of C_{anth} in the South Pacific gyre after 2005 appears very consistent in timing with the strong increase found earlier in the Southern Ocean uptake of CO_2 south of 35°S (the latitudes responsible for the majority of the global air-sea CO_2 flux variability; Gruber, Landschützer, et al., 2019) after 2000, and especially the high rates of uptake after 2009, when this region was taking up more CO_2 from the atmosphere than expected from the increase in atmospheric CO_2 (Feely et al., 2017;

10.1029/2018GB006154

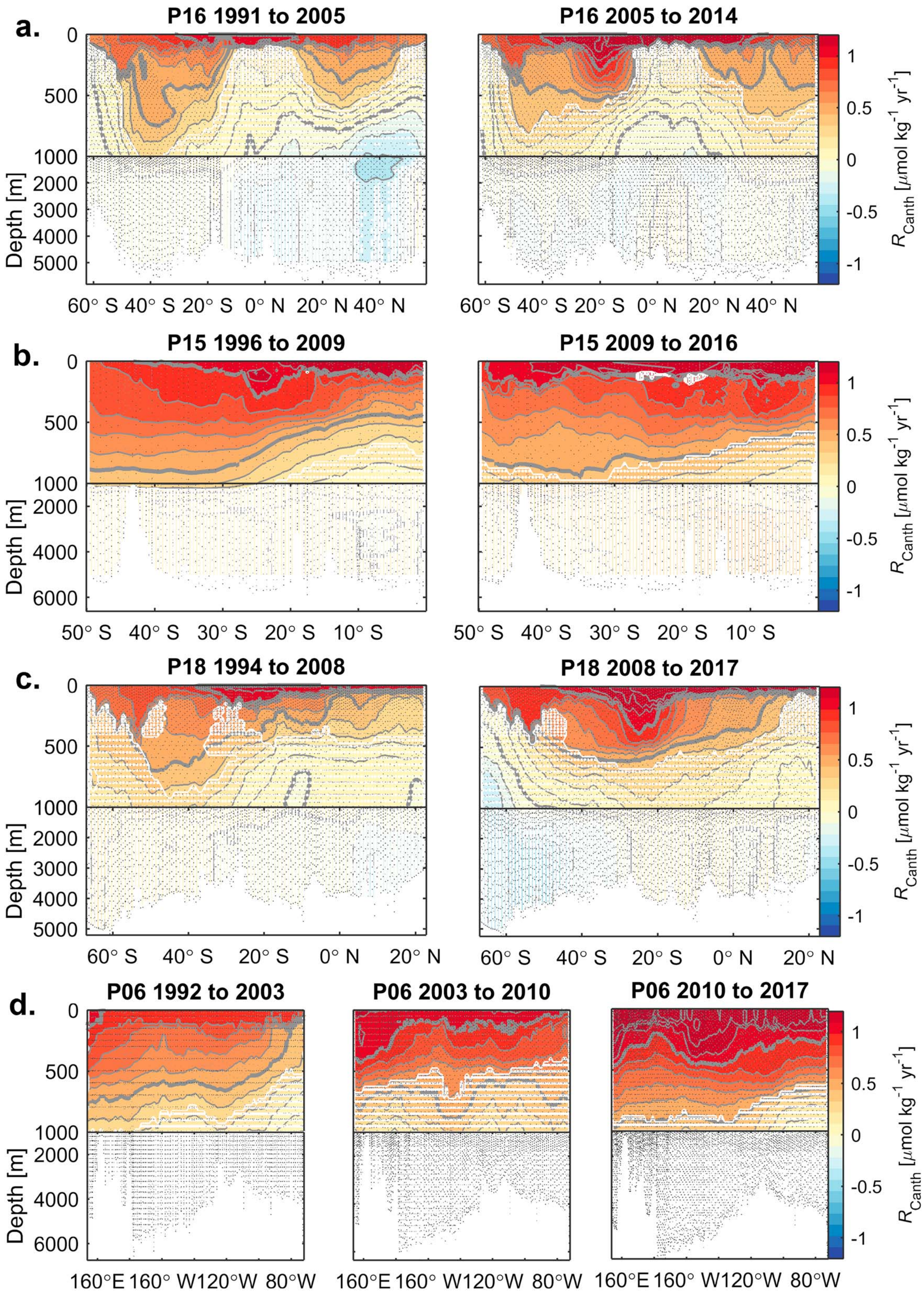

Figure 7. Successive occupation C_{anth} accumulation rates estimated for the meridional (north-south) sections (a) P16 along ~150°W, (b) P15 along ~170°W, (c) P18 along ~103°W to 110°W, and the zonal (east-west) section (d) P06 along 30°S to 33°S (mapped in Figure 1). Time spans of these estimates are given in the panel titles. Estimates with colors covered by white dots are not statistically distinguishable from 0 change to greater than 95% confidence. Small gray and black dots indicate data locations in the earlier and later decades, respectively. Thick gray contours demark every 0.5 μmol/kg beginning at 0, and thinner gray contours demark every 0.1 μmol/kg. Inset maps indicate the section locations.

Gruber, Landschützer, et al., 2019; Landschützer et al., 2015, 2016). We note that these authors use a broad definition of the Southern Ocean that includes the ventilation regions for much of the southern Pacific Subtropical Gyre thermocline, and our results show that shallower subtropical gyre thermocline ventilation may be at least as important for decadal C_{anth} variability as thermocline ventilation by mode and intermediate waters (Figure 7). Thus, it appears as if at least some part of the increase in the Southern Ocean CO_2 uptake from the atmosphere was also driven by an anomalous uptake of C_{anth}. A zeroth-order estimate of this contribution can be obtained by comparing uptake and accumulation accelerations over the basin scale; the large spatial scales considered should reduce the impacts of DIC redistribution from interior ocean mixing. Landschützer et al. (2016)'s flux product suggests that the Pacific Ocean (as we have defined it) took up 2.7 PgC more CO_2 in the 2005-to-2015 decade than in the 1995-to-2005 decade. This is indistinguishable from our estimate of 2.9 (±1.6) PgC acceleration from C_{anth}. This implies that we can account for more or less the entire acceleration in Pacific CO_2 uptake through an increase in the uptake of C_{anth}, most likely driven partially by changes in circulation. Thus, our observations imply a substantially larger contribution of C_{anth} variability to the total air-sea CO_2 flux variability than was suggested by DeVries et al. (2017).

DeVries et al. (2017) suggest that global C_{anth} accumulation was unusually slow from 2000 to 2010 due to sluggish upper ocean overturning circulation. A direct comparison of our accumulation estimates with the results of DeVries et al. (2017) is not possible because of the 5-year shift between the time periods we and they consider and the limitation that neither of our methods can resolve variability within time spans. However, their findings are broadly consistent with our finding of slower C_{anth} accumulation in the subtropical South Pacific in the periods prior to the 2005 (P16), 2008 (P18), 2009 (P15), and 2010 (P06) cruises compared to afterward. If we shift our LIR regression time spans to the periods before and after 2000 (instead of 2005; see section 3.4) and (as DeVries et al., 2017, did) use no data collected after late 2013, then our accumulation rate estimate for the period after 2000 is a slow 7.9 (±1.1) PgC per decade. This accumulation rate rebounds to a number essentially identical to our accumulation rate for 2005 to 2015 of 11.6 (±1.1) PgC per decade if we include the new section occupations since 2014 (including five in the Southern Pacific: P15, P16, P18, P06, and S04P). This suggests that the strong recent accumulation was not visible in the older data used by DeVries et al. (2017). The absence of data prior to the early/middle 1990s means that our estimates for 1990 to 2000 are not as accurate, but we note that these estimates are always greater than our estimates for 1995 to 2005. Collectively, these observations suggest that ~1995 to 2010 was a period of comparatively slow C_{anth} accumulation with faster accumulation occurring both before and since then. DeVries et al. (2017) attribute a −0.9 PgC decade^{-2} ocean C_{anth} uptake deceleration across the Pacific Basin to circulation variability between the 1990s and the 2000s, which is comparable in magnitude to our 1.5 (±1.6) PgC decade^{-2} estimate of the recent (after 2005) rebound in accumulation (with the caveat that this is a comparison between basin uptake and accumulation and does not account for transport into or out of the domain). Interestingly, DeVries et al. (2017) found circulation pattern anomalies in the 1990s (see their extended data Figure 2) that fit spatially with the basin-integrated accumulation rate changes we see after 2005 (supporting information Figure S4), notably including increased Southern Ocean overturning and stronger ventilation of the Southern Hemisphere's shallow thermocline (15°S to 35°S, 100- to 500-m depth).

C_{anth} accumulation below ~200-m depth in the Pacific Ocean is higher between 2005 and 2015 compared to the earlier decade and lower closer to the surface. Even though these changes are not statistically significant yet (supporting information Figure S5b), this pattern is consistent with a gradual penetration of the anthropogenic transient into the deeper reaches of the subtropical thermoclines and with a diminishing capacity of the surface ocean to store additional C_{anth} as Revelle Factors increase along with surface pCO_2 (Revelle, 1934). The mean C_{anth} penetration depth (Broecker et al., 1979) was 349 m in 1995, 355 m in 2005, and 372 m in 2015 based on our analysis. The larger penetration depth increase in the recent decade represents a departure from steady state evolution of an exponential transient signal and supports the idea of a circulation-driven change in accumulation between 2005 and 2015 (Gammon et al., 1982). Changes in ventilation resulting from physical circulation variability challenge the interpretation of eMLR results as purely C_{anth} signals since this variability could result in nonstationary relationships between seawater properties (Goodkin et al., 2011). Nevertheless, the uncertainty analysis (supporting information S1) shows that such violations of eMLR assumptions are a small component of the C_{anth} estimate uncertainty.

10.1029/2018GB006154

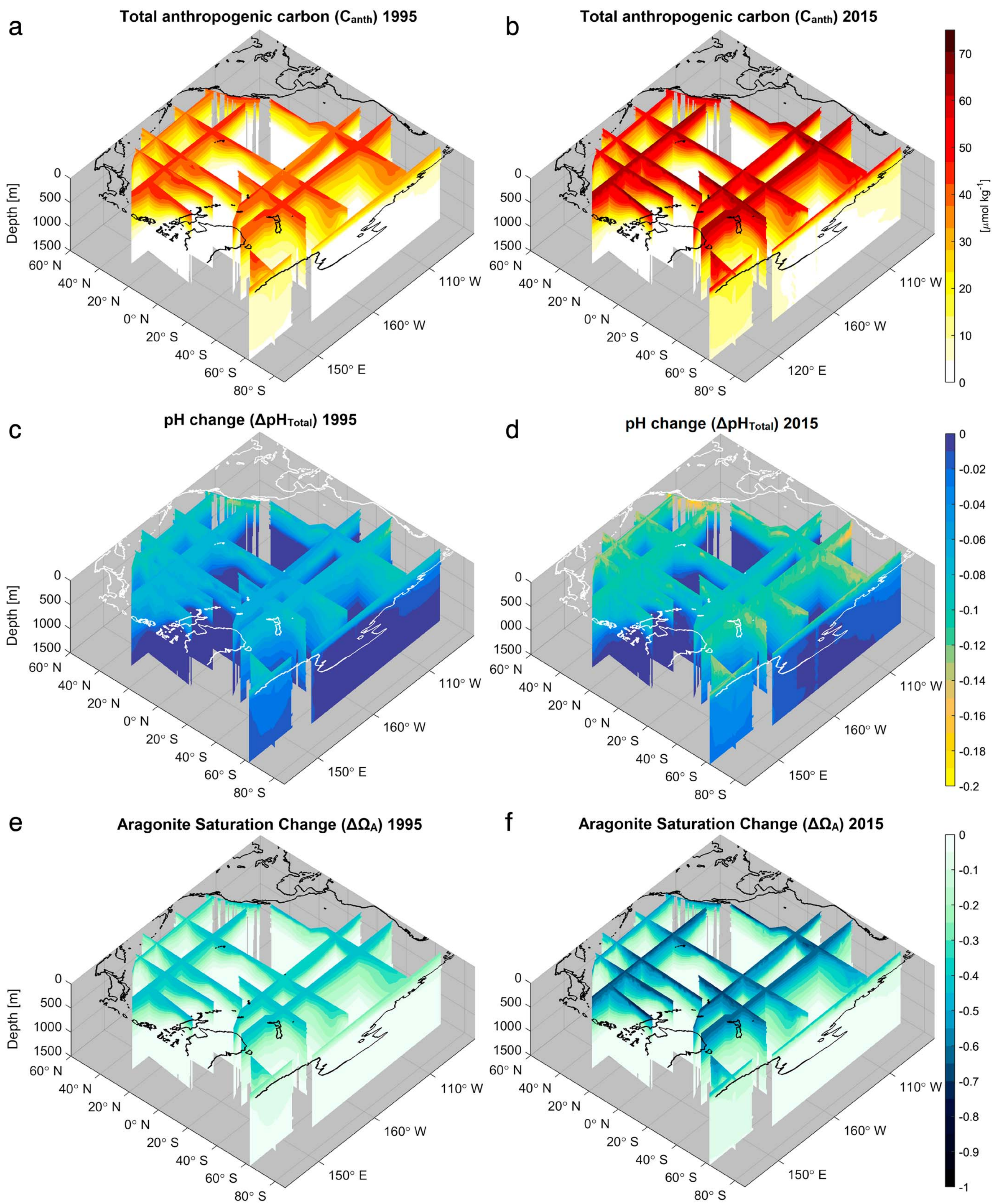

Figure 8. Total C_{anth} estimated in 1995 and 2015 (a, b) and the impact of this C_{anth} on (c, d) pH (ΔpH) and (e, f) the aragonite saturation state Ω (ΔΩ) along all 14 sections considered across the Pacific. Animated versions of these figures are available as supporting information.

3.5. Impacts of C_{anth} on Seawater Chemistry

The impacts of C_{anth} on aragonite mineral saturation state Ω closely resemble the C_{anth} distributions, with the highest C_{anth} concentrations (~50 μmol/kg in 1995 and >65 μmol/kg in 2015) near the surface and in the subtropical gyre thermoclines matching the largest decreases in Ω (~0.5 in 1995 and >0.65 in 2015: Figure 8). In contrast, calculated ΔpH typically has a subsurface maximum absolute change where there is no corresponding C_{anth} maximum (with typically ~0.005 to 0.015 greater pH decreases at ~200-m depth than at the surface). The ΔpH maxima are found between the ocean surface where the C_{anth} concentrations are highest and the deeper old remineralized-DIC-rich waters where C_{anth} concentrations are lower, but the impact of C_{anth} on pH (closely related to the Revelle factor) is at a maximum (Feely et al., 2009). Similarly, the impacts of surface C_{anth} on pH are greatest in the colder, higher Revelle factor, high-latitude waters (Egleston et al., 2010, with 0.04 larger surface pH decreases at high latitudes being common). The subsurface ΔpH maxima are especially pronounced in upwelling areas such as off the U.S. West Coast where cold very high DIC waters are brought near the ocean surface (with pH decreases as large as −0.125 in 1995 and −0.185 in 2015). C_{anth} estimates for 1995, 2005 (not shown), and 2015 are interpolated or extrapolated in time (see section 3.4) to produce visualizations of C_{anth} accumulation and its impacts on pH and Ω (additional supporting information).

4. Summary

We present updated estimates of Pacific C_{anth} inventories and accumulation rates determined using updates to the eMLR approach combining several recommendations from the literature (Carter, Feely, Williams, et al., 2017; Clement & Gruber, 2018; Thacker, 2012). Our estimates are obtained by comparing measurements from a section to measurements from subsequent occupations of that same section. Our efforts take advantage of the fact that GO-SHIP has recently completed the second, third, or fourth occupations of most of the 14 sections used in this study.

C_{anth} accumulation, storage, and inventories are estimated for a range of locations, depths, and latitude bands. A central finding is that the Pacific C_{anth} accumulation rate increased from 8.8 (±1.1, uncertainties at 1σ) PgC per decade between 1995 and 2005 to 11.7 (±1.1) PgC per decade between 2005 and 2015. The majority of this ocean C_{anth} increase occurs in response to the large and growing burden of C_{anth} in the atmosphere. However, we find that the variability in this ocean C_{anth} sink can be attributed to both atmospheric C_{anth} accumulation and ocean circulation and ventilation variability: the observed acceleration of 2.9 (±1.6) PgC decade^{-2} is larger than the 1.4 (±0.4) PgC decade^{-2} acceleration expected from increasing atmospheric C_{anth}, though only significantly larger across the Southern Pacific Gyre where 2.1 (±0.6) PgC decade^{-2} of a 2.6 (±0.6) PgC decade^{-2} acceleration is not attributed to atmospheric accumulation. Our data synthesis is consistent with literature indicating a recent spin-up of Southern Hemisphere Subtropical Gyre circulation. We suggest that these circulation changes have led to an increase in ocean C_{anth} storage beyond that expected from atmospheric C_{anth} accumulation and that this enhanced C_{anth} storage is, at least in part, a consequence of the recent reinvigoration of the global ocean carbon uptake—predominantly south of 35°S—that has been noted in literature.

Accumulation rates are significant over the top 1,500 m of the Pacific and tend to be greatest in warmer, lighter waters that have lower Revelle Factors and are in close contact with the atmosphere. In the interior, C_{anth} accumulation extends deepest nearer the intermediate and mode water formation areas located along the boundaries between the subtropical and subpolar gyres and in the western portions of the subtropical gyres where the thermocline extends deepest (with surface convergence centered around 30°S and 30°N for the Southern and Northern Hemisphere Gyres, respectively; e.g., Lumpkin & Johnson, 2013). Upwelling and surface divergence near the equator (particularly in the Eastern Tropical Pacific), in the subpolar North Pacific, in the Southern Ocean, and along the eastern boundary current of the California Current System displace well-ventilated water with deeper water with less C_{anth}, leading to lower accumulation rates and smaller inventory increases in these regions. However, accumulation rates are increasing in recent years in the equatorial latitudes where C_{anth} reemerges (Toyama et al., 2017). Our findings are consistent also with recent findings of decadal C_{anth} accumulation in bottom waters originating from the

Southern Ocean, though extending this analysis to other sections crossing the Indian and Atlantic sectors of the Southern Ocean would improve confidence in this observation.

A comparison of the magnitudes of the C_{anth} accumulation rate estimates to their declining uncertainties suggests that continuing repeat hydrographic reoccupations with the highest quality measurements and a comparably dense sampling plan will be essential for continued monitoring of decadal C_{anth} accumulation in the ocean and its roles in modulating atmospheric CO_2 increase and driving ocean acidification.

Acknowledgments
The data we use can be accessed at CCHDO website (https://cchdo.ucsd.edu/) and GLODAP website (https://www.glodap.info/). This research would not be possible without the hard work of the scientists and crew aboard the many repeated hydrographic cruises coordinated by GO-SHIP, which is funded by NSF OCE and NOAA OAR. We thank funding agencies and program managers as follows: U.S., Australian, Japanese national science funding agencies that support data collection, data QA/QC, and data centers. Contributions from B. R. C., R. A. F., and R. W. are supported by the National Oceanic and Atmospheric Administration Global Ocean Monitoring and Observing Program (Data Management and Synthesis Grant: N8R3CEA-PDM managed by Kathy Tedesco and David Legler). G. C. J. is supported by the Climate Observation Division, Climate Program Office, National Oceanic and Atmospheric Administration (NOAA), U.S. Department of Commerce and NOAA Research (fund reference 100007298), grant (N8R1SE3-PGC). B. M. S was supported by the Australian Government Department of the Environment and CSIRO through the Australian Climate Change Science Programme and by the National Environmental Science Program. N. G. acknowledges support by ETH Zurich. This is JISAO contribution 2018-0149 and PMEL contribution 4786. We fondly remember John Bullister as a treasured friend, valued colleague, and dedicated mentor, and we thank him for sharing his days with us. He is and will be dearly missed.

References

Anderson, L. A., & Sarmiento, J. L. (1994). Redfield ratios of remineralization determined by nutrient data analysis. *Global Biogeochem Cycles*, *8*(1), 65–80. https://doi.org/10.1029/93GB03318

Bates, N., Astor, Y., Church, M., Currie, K., Dore, J., Gonaález-Dávila, M., et al. (2014). A Time-Series View of Changing Ocean Chemistry Due to Ocean Uptake of Anthropogenic CO_2 and Ocean Acidification. *Oceanography*, *27*(1), 126–141. https://doi.org/10.5670/oceanog.2014.16

Broecker, W. S., Takahashi, T., Simpson, H. J., & Peng, T. H. (1979). Fate of fossil fuel carbon dioxide and the global carbon budget. *Science*, *206*(4417), 409–418. https://doi.org/10.1126/science.206.4417.409

Caldeira, K., & Wickett, M. E. (2005). Ocean model predictions of chemistry changes from carbon dioxide emissions to the atmosphere and ocean. *Journal of Geophysical Research*, *110*, C09S04. https://doi.org/10.1029/2004JC002671

Carter, B. R., Feely, R. A., Mecking, S., Cross, J. N., Macdonald, A. M., Siedlecki, S. A., et al. (2017). Two decades of Pacific anthropogenic carbon storage and ocean acidification along Global Ocean Ship-based Hydrographic Investigations Program sections P16 and P02. *Global Biogeochem Cycles*, *31*, 306–327. https://doi.org/10.1002/2016GB005485

Carter, B. R., Feely, R. A., Williams, N. L., Dickson, A. G., Fong, M. B., & Takeshita, Y. (2017). Updated methods for global locally interpolated estimation of alkalinity, pH, and nitrate. *Limnology and Oceanography: Methods*, *16*(2), 119–131. https://doi.org/10.1002/lom3.10232

Chu, S. N., Wang, Z. A., Doney, S. C., Lawson, G. L., & Hoering, K. A. (2016). Changes in anthropogenic carbon storage in the Northeast Pacific in the last decade. *Journal of Geophysical Research: Oceans*, *121*, 4618–4632. https://doi.org/10.1002/2016JC011775

Ciais, P., Tan, J., Wang, X., Roedenbeck, C., Chevallier, F., Piao, S. L., et al. (2019). Five decades of northern land carbon uptake revealed by the interhemispheric CO_2 gradient. *Nature*, *568*(7751), 221–225. https://doi.org/10.1038/s41586-019-1078-6

Clement, D., & Gruber, N. (2018). The eMLR(C*) method to determine decadal changes in the global ocean storage of anthropogenic CO_2. *Global Biogeochemical Cycles*, *32*, 654–679. https://doi.org/10.1002/2017GB005819

DeVries, T., Holzer, M., & Primeau, F. (2017). Recent increase in oceanic carbon uptake driven by weaker upper-ocean overturning. *Nature*, *542*(7640), 215–218. https://doi.org/10.1038/nature21068

Doney, S. C., Fabry, V. J., Feely, R. A., & Kleypas, J. A. (2009). Ocean acidification: The other CO_2 problem. *Annual Review of Marine Science*, *1*(1), 169–192. https://doi.org/10.1146/annurev.marine.010908.163834

Egleston, E. S., Sabine, C. L., & Morel, F. M. M. (2010). Revelle revisited: Buffer factors that quantify the response of ocean chemistry to changes in DIC and alkalinity. *Global Biogeochemical Cycles*, *24*, GB1002. https://doi.org/10.1029/2008GB003407

England, M. H. (1995). The age of water and ventilation timescales in a global ocean model. *Journal of Physical Oceanography*, *25*(11), 2756–2777. https://doi.org/10.1175/1520-0485(1995)025<2756:TAOWAV>2.0.CO;2

England, M. H., McGregor, S., Spence, P., Meehl, G. A., Timmermann, A., Cai, W., et al. (2014). Recent intensification of wind-driven circulation in the Pacific and the ongoing warming hiatus. *Nature Climate Change*, *4*(3), 222–227. https://doi.org/10.1038/nclimate2106

Feely, R., Doney, S., & Cooley, S. (2009). Ocean acidification: Present conditions and future changes in a high-CO_2 world. *Oceanography*, *22*(4), 36–47. https://doi.org/10.5670/oceanog.2009.95

Feely, R. A., Wanninkhof, P., Landschützer, R., Carter, B. R., & Triñanes, J. A. (2017). Ocean carbon. In State of the Climate in 2016. *Bulletin of the American Meteorological Society*, *98*(8), Si–S280. https://doi.org/10.1175/2017BAMSStateoftheClimate.1

Friis, K., Körtzinger, A., Pätsch, J., & Wallace, D. W. R. (2005). On the temporal increase of anthropogenic $_2$ in the subpolar North Atlantic. *Deep-Sea Research Part I: Oceanographic Research Papers*, *52*(5), 681–698. https://doi.org/10.1016/j.dsr.2004.11.017

Gammon, R. H., Cline, J., & Wisegarver, D. (1982). Chlorofluoromethanes in the northeast Pacific Ocean: Measured vertical distributions and application as transient tracers of upper ocean mixing. *Journal of Geophysical Research*, *87*(C12), 9441–9454. https://doi.org/10.1029/JC087iC12p09441

Gattuso, J.-P., Magnan, A., Billé, R., Cheung, W. W. L., Howes, E. L., Joos, F., et al. (2015). Contrasting futures for ocean and society from different anthropogenic CO_2 emissions scenarios. *Science*, *349*(6243), aac4722. https://doi.org/10.1126/science.aac4722

Gloor, M., Gruber, N., Sarmiento, J., Sabine, C. L., Feely, R. A., & Rödenbeck, C. (2003). A first estimate of present and preindustrial air-sea CO_2 flux patterns based on ocean interior carbon measurements and models. *Geophysical Research Letters*, *30*(1), 1010. https://doi.org/10.1029/2002GL015594

Goodkin, N. F., Levine, N. M., Doney, S. C., & Wanninkhof, R. (2011). Impacts of temporal CO_2 and climate trends on the detection of ocean anthropogenic CO_2 accumulation. *Global Biogeochem Cycles*, *25*, GB3023. https://doi.org/10.1029/2010GB004009

Gordon, A. L., Huber, B. A., & Busecke, J. (2015). Bottom water export from the western Ross Sea, 2007 through 2010. *Geophysical Research Letters*, *42*, 5387–5394. https://doi.org/10.1002/2015GL064457

Gruber, N., Clement, D., Carter, B. R., Feely, R. A., van Heuven, S., Hoppema, M., et al. (2019). The oceanic sink for anthropogenic CO_2 from 1994 to 2007. *Science*, *363*(6432), 1193–1199. https://doi.org/10.1126/SCIENCE.AAU5153

Gruber, N., Landschützer, P., & Lovenduski, N. S. (2019). The variable Southern Ocean carbon sink. *Annual Review of Marine Science*, *11*(1), 159–186. https://doi.org/10.1146/annurev-marine-121916-063407

Gruber, N., Sarmiento, J. L., & Stocker, T. F. (1996). An improved method for detecting anthropogenic CO_2 in the oceans. *Global Biogeochem Cycles*, *10*(4), 809–837. https://doi.org/10.1029/96GB01608

Holte, J., Talley, L. D., Gilson, J., & Roemmich, D. (2017). An Argo mixed layer climatology and database. *Geophysical Research Letters*, *44*, 5618–5626. https://doi.org/10.1002/2017GL073426

Johnson, G. C. (2008). Quantifying Antarctic bottom water and North Atlantic deep water volumes. *Journal of Geophysical Research*, *113*, C05027. https://doi.org/10.1029/2007JC004477

Katsumata, K., Nakano, H., & Kumamoto, Y. (2015). Dissolved oxygen change and freshening of Antarctic Bottom water along 62°S in the Australian-Antarctic Basin between 1995/1996 and 2012/2013. *Deep-Sea Research Part II: Topical Studies in Oceanography*, *114*, 27–38. https://doi.org/10.1016/J.DSR2.2014.05.016

Key, R. M., Kozyr, A., Sabine, C. L., Lee, K., Wanninkhof, R., Bullister, J. L., et al. (2004). A global ocean carbon climatology: Results from Global Data Analysis Project (GLODAP). *Global Biogeochem Cycles*, *18*, GB4031. https://doi.org/10.1029/2004GB002247

Kouketsu, S., Murata, A., & Doi, T. (2013). Decadal changes in dissolved inorganic carbon in the Pacific Ocean. *Global Biogeochem Cycles*, *27*, 65–76. https://doi.org/10.1029/2012GB004413

Kouketsu, S., & Murata, A. M. (2014). Detecting decadal scale increases in anthropogenic CO_2 in the ocean. *Geophysical Research Letters*, *41*, 4594–4600. https://doi.org/10.1002/2014GL060516

Landschützer, P., Gruber, N., & Bakker, D. C. E. (2016). Decadal variations and trends of the global ocean carbon sink. *Global Biogeochem Cycles*, *30*, 1396–1417. https://doi.org/10.1002/2015GB005359

Landschützer, P., Gruber, N., Haumann, F. A., Rödenbeck, C., Bakker, D. C. E., van Heuven, S., et al. (2015). The reinvigoration of the Southern Ocean carbon sink. *Science*, *349*(6253), 1221–1224. https://doi.org/10.1126/science.aab2620

Le Quéré, C., Andrew, R. M., Canadell, J. G., Sitch, S., Korsbakken, J. I., Peters, G. P., et al. (2016). Global carbon budget 2016. *Earth System Science Data*, *8*(2), 605–649. https://doi.org/10.5194/essd-8-605-2016

Le Quéré, C., Moriarty, R., Andrew, R. M., Canadell, J. G., Sitch, S., Korsbakken, J. I., et al. (2015). Global carbon budget 2015. *Earth System Science Data*, *7*(2), 349–396. https://doi.org/10.5194/essd-7-349-2015

Lee, K., Kim, T.-W., Byrne, R. H., Millero, F. J., Feely, R. A., & Liu, Y.-M. (2010). The universal ratio of boron to chlorinity for the North Pacific and North Atlantic oceans. *Geochimica et Cosmochimica Acta*, *74*(6), 1801–1811. https://doi.org/10.1016/j.gca.2009.12.027

Li, H., & Ilyina, T. (2018). Current and future decadal trends in the oceanic carbon uptake are dominated by internal variability. *Geophysical Research Letters*, *45*, 916–925. https://doi.org/10.1002/2017GL075370

Locarnini, R. A., A. V. Mishonov, J. I. Antonov, T. P. Boyer, H. E. Garcia, O. K. Baranova, et al. (2013). *World ocean atlas 2013. Vol. 1: Temperature*. In S. Levitus (Ed.), A. Mishonov (Technical Ed.), NOAA Atlas NESDIS (*73*, pp. 40). Silver Spring, MD. https://doi.org/10.7289/V55X26VD

Loeb, N. G., Lyman, J. M., Johnson, G. C., Allan, R. P., Doelling, D. R., Wong, T., et al. (2012). Observed changes in top-of-the-atmosphere radiation and upper-ocean heating consistent within uncertainty. *Nature Geoscience*, *5*(2), 110–113. https://doi.org/10.1038/ngeo1375

Lueker, T. J., Dickson, A. G., & Keeling, C. D. (2000). Ocean pCO_2 calculated from dissolved inorganic carbon, alkalinity, and equations for K1 and K2: Validation based on laboratory measurements of CO_2 in gas and seawater at equilibrium. *Marine Chemistry*, *70*(1–3), 105–119. https://doi.org/10.1016/S0304-4203(00)00022-0

Lumpkin, R., & Johnson, G. C. (2013). Global ocean surface velocities from drifters: Mean, variance, El Niño-Southern Oscillation response, and seasonal cycle. *Journal of Geophysical Research: Oceans*, *118*, 2992–3006. https://doi.org/10.1002/jgrc.20210

McNeil, B. I., Tilbrook, B., & Matear, R. J. (2001). Accumulation and uptake of anthropogenic CO_2 in the Southern Ocean, south of Australia between 1968 and 1996. *Journal of Geophysical Research*, *106*(C12), 31,431–31,445. https://doi.org/10.1029/2000JC000331

McPhaden, M. J., & Zhang, D. (2004). Pacific Ocean circulation rebounds. *Geophysical Research Letters*, *31*, L18301. https://doi.org/10.1029/2004GL020727

Mikaloff Fletcher, S. E., Gruber, N., Jacobson, A. R., Doney, S. C., Dutkiewicz, S., Gerber, M., et al. (2006). Inverse estimates of anthropogenic CO_2 uptake, transport, and storage by the ocean. *Global Biogeochem Cycles*, *20*, GB2002. https://doi.org/10.1029/2005GB002530

Murata, A., Kumamoto, Y., & Sasaki, K. (2019). Decadal-scale increases of anthropogenic CO_2 in Antarctic bottom water in the Indian and Western Pacific sectors of the Southern Ocean. *Geophysical Research Letters*, *46*, 833–841. https://doi.org/10.1029/2018GL080604

Murata, A., Kumamoto, Y., Sasaki, K., Watanabe, S., & Fukasawa, M. (2009). Decadal increases of anthropogenic CO_2 along149°E in the western North Pacific. *Journal of Geophysical Research*, *114*(C4), C04018. https://doi.org/10.1029/2008JC004920

Murata, A., Kumamoto, Y., Watanabe, S., & Fukasawa, M. (2007). Decadal increases of anthropogenic CO_2 in the South Pacific subtropical ocean along 32°S. *Journal of Geophysical Research*, *112*, C05033. https://doi.org/10.1029/2005JC003405

Olsen, A., Key, R. M., van Heuven, S., Lauvset, S. K., Velo, A., Lin, X., et al. (2016). The global ocean data analysis project version 2 (GLODAPv2)—An internally consistent data product for the world ocean. *Earth System Science Data*, *8*(2), 297–323. https://doi.org/10.5194/essd-8-297-2016

Orr, J. C., Epitalon, J. M., & Gattuso, J. P. (2015). Comparison of ten packages that compute ocean carbonate chemistry. *Biogeosciences*, *12*(5), 1483–1510. https://doi.org/10.5194/bg-12-1483-2015

Orr, J. C., Fabry, V. J., Aumont, O., Bopp, L., Doney, S. C., Feely, R. A., et al. (2005). Anthropogenic ocean acidification over the twenty-first century and its impact on calcifying organisms. *Nature*, *437*(7059), 681–686. https://doi.org/10.1038/nature04095

Orr, J. C., Maier-Reimer, E., Mikolajewicz, U., Monfray, P., Sarmiento, J. L., Toggweiler, J. R., et al. (2001). Estimates of anthropogenic carbon uptake from four three-dimensional global ocean models. *Global Biogeochem Cycles*, *15*(1), 43–60. https://doi.org/10.1029/2000GB001273

Orsi, A. H., Johnson, G. C., & Bullister, J. L. (1999). Circulation, mixing, and production of Antarctic Bottom Water. *Progress in Oceanography*, *43*(1), 55–109. https://doi.org/10.1016/S0079-6611(99)00004-X

Pardo, P. C., Tilbrook, B., Langlais, C., Trull, T. W., & Rintoul, S. R. (2017). Carbon uptake and biogeochemical change in the Southern Ocean, south of Tasmania. *Biogeosciences*, *14*(22), 5217–5237. https://doi.org/10.5194/bg-14-5217-2017

Peng, T.-H., Wanninkhof, R., & Feely, R. A. (2003). Increase of anthropogenic CO_2 in the Pacific Ocean over the last two decades. *Deep-Sea Research Part II: Topical Studies in Oceanography*, *50*(22–26), 3065–3082. https://doi.org/10.1016/J.DSR2.2003.09.001

Plancherel, Y., Rodgers, K., Key, R., Jacobson, A., & Sarmiento, J. (2013). Role of regression model selection and station distribution on the estimation of oceanic anthropogenic carbon change by eMLR. *Biogeosciences*, *10*(7), 4801–4831. https://doi.org/10.5194/bg-10-4801-2013

Purkey, S. G., & Johnson, G. C. (2013). Antarctic bottom water warming and freshening: Contributions to sea level rise, ocean freshwater budgets, and global heat gain. *Journal of Climate*, *26*(16), 6105–6122. https://doi.org/10.1175/JCLI-D-12-00834.1

Qu, T., Gao, S., Fine, R. A., Qu, T., Gao, S., & Fine, R. A. (2013). Subduction of South Pacific tropical water and its equatorward pathways as shown by a simulated passive tracer*. *Journal of Physical Oceanography*, *43*(8), 1551–1565. https://doi.org/10.1175/JPO-D-12-0180.1

Quay, P., Sonnerup, R., Stutsman, J., Maurer, J., Körtzinger, A., Padin, X. A., & Robinson, C. (2007). Anthropogenic CO_2 accumulation rates in the North Atlantic Ocean from changes in the $^{13}C/^{12}C$ of dissolved inorganic carbon. *Global Biogeochem Cycles*, *21*, GB1009. https://doi.org/10.1029/2006GB002761

Revelle, R. (1934). Physico-chemical factors affecting the solubility of calcium carbonate in sea water. *Journal of Sedimentary Petrology*, *4*(3), 103–110. https://doi.org/10.1306/D4268ED2-2B26-11D7-8648000102C1865D

Ríos, A. F., Velo, A., Pardo, P. C., Hoppema, M., & Pérez, F. F. (2012). An update of anthropogenic CO_2 storage rates in the western South Atlantic basin and the role of Antarctic Bottom Water. *Journal of Marine Systems*, *94*, 197–203. https://doi.org/10.1016/J.JMARSYS.2011.11.023

Rintoul, S. R. (1998). On the origin and influence of Adélie land bottom water. In S. Jacobs, & R. Weiss (Eds.), *Ocean, Ice and Atmosphere: Interaction at the Antarctic Continental Margin*, (Vol. 75, pp. 151–171). Washington, DC: American Geophysical Union. https://doi.org/10.1029/AR075p0151

Roemmich, D., Gilson, J., Davis, R., Sutton, P., Wijffels, S., & Riser, S. (2007). Decadal Spinup of the South Pacific Subtropical Gyre. *Journal of Physical Oceanography*, *37*(2), 162–173. https://doi.org/10.1175/JPO3004.1

Roemmich, D., Gilson, J., Sutton, P., Zilberman, N., Roemmich, D., Gilson, J., et al. (2016). Multidecadal change of the South Pacific gyre circulation. *Journal of Physical Oceanography*, *46*(6), 1871–1883. https://doi.org/10.1175/JPO-D-15-0237.1

Sabine, C. L., Feely, R. A., Gruber, N., Key, R. M., Lee, K., Bullister, J. L., et al. (2004). The oceanic sink for anthropogenic CO_2. *Science*, *305*(5682), 367–371. https://doi.org/10.1126/science.1097403

Sabine, C. L., Feely, R. A., Key, R. M., Bullister, J. L., Millero, F. J., Lee, K., et al. (2002). Distribution of anthropogenic CO_2 in the Pacific Ocean. *Global Biogeochemical Cycles*, *16*(4), 1083. https://doi.org/10.1029/2001GB001639

Sabine, C. L., Feely, R. A., Millero, F. J., Dickson, A. G., Langdon, C., Mecking, S., & Greeley, D. (2008). Decadal changes in Pacific carbon. *Journal of Geophysical Research*, *113*, C07021. https://doi.org/10.1029/2007JC004577

Sabine, C. L., Key, R. M., Johnson, K. M., Millero, F. J., Poisson, A., Sarmiento, J. L., et al. (1999). Anthropogenic CO_2 inventory of the Indian Ocean. *Global Biogeochem Cycles*, *13*(1), 179–198. https://doi.org/10.1029/1998GB900022

Sarmiento, J. L., & Le Quéré, C. (1996). Oceanic carbon dioxide uptake in a model of century-scale global warming. *Science*, *274*(5291), 1346–1350. https://doi.org/10.1126/SCIENCE.274.5291.1346

Sarmiento, J. L., Orr, J. C., & Siegenthaler, U. (1992). A perturbation simulation of CO_2 uptake in an ocean general circulation model. *Journal of Geophysical Research*, *97*(C3), 3621–3645. https://doi.org/10.1029/91JC02849

Slansky, C. M., Feely, R. A., & Wanninkhof, R. (1997). The stepwise linear regression method for calculating anthropogenic CO_2 invasion into the north Pacific Ocean. In *Biogeochemical Processes in the North Pacific, Proceedings of the International Marine Science Symposium on Biogeochemical Processes in the North Pacific* (pp. 70–79). Mutsu, Japan: Japan Marine Science Foundation.

Sutton, A. J., Wanninkhof, R., Sabine, C. L., Feely, R. A., Cronin, M. F., & Weller, R. A. (2017). Variability and trends in surface seawater pCO_2 and CO_2 flux in the Pacific Ocean. *Geophysical Research Letters*, *44*, 5627–5636. https://doi.org/10.1002/2017GL073814

Talley, L. D., Feely, R. A., Sloyan, B. M., Wanninkhof, R., Baringer, M. O., Bullister, J. L., et al. (2016). Changes in ocean heat, carbon content, and ventilation: A review of the first decade of GO-SHIP Global repeat hydrography. *Annual Review of Marine Science*, *8*(1), 185–215. https://doi.org/10.1146/annurev-marine-052915-100829

Thacker, W. C. (2012). Regression-based estimates of the rate of accumulation of anthropogenic CO_2 in the ocean: A fresh look. *Marine Chemistry*, *132-133*, 44–55. https://doi.org/10.1016/J.MARCHEM.2012.02.004

Toyama, K., Rodgers, K. B., Blanke, B., Iudicone, D., Ishii, M., Aumont, O., & Sarmiento, J. L. (2017). Large reemergence of anthropogenic carbon into the ocean's surface mixed layer sustained by the ocean's overturning circulation. *Journal of Climate*, *30*(21), 8615–8631. https://doi.org/10.1175/JCLI-D-16-0725.1

Uppström, L. R. (1974). The boron/chlorinity ratio of deep-sea water from the Pacific Ocean. *Deep Sea Research and Oceanographic Abstracts*, *21*(2), 161–162. https://doi.org/10.1016/0011-7471(74)90074-6

van Hueven, S., D. Pierrot, J. W. B. Rae, E. Lewis, and D. W. R. Wallace (2011). MATLAB program developed for CO_2 system calculations, ORNL/CDIAC-105b. Carbon Dioxide Information Analysis Center, Oak Ridge National Laboratory, U.S. Department of Energy, Oak Ridge, Tennessee. https://doi.org/10.3334/CDIAC/otg.CO2SYS_MATLAB_v1.1

Velo, A., Pérez, F. F., Tanhua, T., Gilcoto, M., Ríos, A. F., & Key, R. M. (2013). Total alkalinity estimation using MLR and neural network techniques. *Journal of Marine Systems*, *111-112*, 11–18. https://doi.org/10.1016/j.jmarsys.2012.09.002

Velo, A., Vázquez-Rodríguez, M., Padín, X. A., Gilcoto, M., Ríos, A. F., Pérez, F. F., & Pérez, F. F. (2010). A multiparametric method of interpolation using WOA05 applied to anthropogenic CO_2 in the Atlantic. *Scientia Marina*, *74*(S1), 21–32. https://doi.org/10.3989/scimar.2010.74s1021

Wakita, M., Watanabe, S., Murata, A., Tsurushima, N., & Honda, M. (2010). Decadal change of dissolved inorganic carbon in the subarctic western North Pacific Ocean. *Tellus Series B: Chemical and Physical Meteorology*, *62*(5), 608–620. https://doi.org/10.1111/j.1600-0889.2010.00476.x

Wallace, D. (1995). *Monitoring Global Ocean Carbon Inventories*. College Station, TX: Texas A&M University.

Wallace, D. W. R. (2001). Chapter 6.3 Storage and transport of excess CO_2 in the oceans: The JGOFS/WOCE global CO_2 survey. *Geophysical Journal International*, *77*, 489–521. https://doi.org/10.1016/S0074-6142(01)80136-4

Wang, S., Moore, J. K., Primeau, F. W., & Khatiwala, S. (2012). Simulation of anthropogenic CO_2 uptake in the CCSM3.1 ocean circulation-biogeochemical model: Comparison with data-based estimates. *Biogeosciences*, *9*(4), 1321–1336. https://doi.org/10.5194/bg-9-1321-2012

Waters, J. F., Millero, F. J., & Sabine, C. L. (2011). Changes in South Pacific anthropogenic carbon. *Global Biogeochem Cycles*, *25*, GB4011. https://doi.org/10.1029/2010GB003988

Waugh, D. W., Hall, T. M., Mcneil, B. I., Key, R., & Matear, R. J. (2006). Anthropogenic CO_2 in the oceans estimated using transit time distributions. *Tellus Series B: Chemical and Physical Meteorology*, *58*(5), 376–389. https://doi.org/10.1111/j.1600-0889.2006.00222.x

Williams, N. L., Feely, R. A., Sabine, C. L., Dickson, A. G., Swift, J. H., Talley, L. D., & Russell, J. L. (2015). Quantifying anthropogenic carbon inventory changes in the Pacific sector of the Southern Ocean. *Marine Chemistry*, *174*, 147–160. https://doi.org/10.1016/j.marchem.2015.06.015

Zeebe, R. E. (2012). History of seawater carbonate chemistry, atmospheric CO_2, and ocean acidification. *Annual Review of Earth and Planetary Sciences*, *40*(1), 141–165. https://doi.org/10.1146/annurev-earth-042711-105521

Zweng, M. M., J. R. Reagan, J. I. Antonov, A. V. Mishonov, T. P. Boyer, H. E. Garcia, et al. (2013), *World Ocean Atlas 2013, Volume 2: Salinity*. S. Levitus, Ed., A. Mishonov Technical Ed.; NOAA Atlas NESDIS *74*, 39 pp.

References From the Supporting Information

Dunne, J. P., John, J. G., Adcroft, A. J., Griffies, S. M., Hallberg, R. W., Shevliakova, E., et al. (2012). GFDL's ESM2 Global Coupled Climate–Carbon Earth System Models. Part I: Physical Formulation and Baseline Simulation Characteristics. *Journal of Climate*, *25*(19), 6646–6665. https://doi.org/10.1175/JCLI-D-11-00560.1

Dunne, J. P., John, J. G., Shevliakova, E., Stouffer, R. J., Krasting, J. P., Malyshev, S. L., et al. (2013). GFDL's ESM2 Global Coupled Climate–Carbon Earth System Models. Part II: Carbon System Formulation and Baseline Simulation Characteristics. *Journal of Climate*, *26*(7), 2247–2267. https://doi.org/10.1175/JCLI-D-12-00150.1

Key, R. M., Tanhua, T., Olsen, A., Hoppema, M., Jutterström, S., Schirnick, C., et al. (2010). The CARINA data synthesis project: Introduction and overview. *Earth System Science Data*, *2*(1), 105–121. https://doi.org/10.5194/essd-2-105-2010

Khatiwala, S. (2007). A computational framework for simulation of biogeochemical tracers in the ocean. *Global Biogeochemical Cycles*, *21*, GB3001. https://doi.org/10.1029/2007GB002923

Lauvset, S. K., Key, R. M., Olsen, A., van Heuven, S., Velo, A., Lin, X., et al. (2016). A new global interior ocean mapped climatology: The 1° × 1° GLODAP version 2. *Earth System Science Data*, *8*(2), 325–340. https://doi.org/10.5194/ESSD-8-325-2016